THE EFFECTIVNESS OF USING A NON-PLATINUM MATERIAL COMBINATION FOR THE CATALYST LAYER OF A PROTON EXCHANGE MEMBRANE FUEL CELL

Dwayne Jensen Reddy

20416564

A dissertation submitted in the fulfilment of the requirements for the Master of Engineering: Electrical

Department: Electrical Power Engineering

Faculty of Engineering

Durban University of Technology

Supervisor: Mr F d'Almaine

Date: October 2015

Declaration

I, Dwayne Jensen Reddy hereby declare that the following research information is solely my own work. This is submitted in fulfilment of the requirements of the Master of Engineering: Department of Electrical Power Engineering at the Durban University of Technology. It has not been submitted for any form of assessment to any other educational institution.

………………………..

Dwayne Jensen Reddy

Date:………………..

Acknowledgements

I hereby wish to express my gratitude to the following individuals who enabled this document to be completed successfully:

- Dr L Jarvis for his guidance and support throughout this research
- Mr F d'Almaine and Mr E.R Bussy for their assistance and encouragement throughout this research
- Eskom Power Plant Engineering Institute (EPPEI) Funding
- Personnel from the Material Science Laboratory at the University of Kwa-Zulu Natal

Dedication

This dissertation is dedicated to my parents, Madhu and Sylvie, to my sister Sanchia and to my partner Serona for their love and motivation during this research project.

Abstract

The effectiveness of using a low cost non - platinum (Pt) material for the catalyst layer of a polymer electrolyte fuel cell (PEMFC) was investigated. A test cell and station was developed. Two commercial Pt loaded membrane electrode assemblies (MEA) and one custom MEA were purchased from the Fuelcelletc store. Hydrogen and oxygen were applied to either side of the custom MEA which resulted in an additional sample tested. An aluminium flow field plate with a hole type design was manufactured for the reactants to reach the reaction sites. End plates made from perspex where used to enclose the MEA, flow field plates, and also to provide reactant inlet and outlet connection points.

The developed test station consisted of hydrogen and oxygen sources, pressure regulators, mass flow controllers, heating plate, and humidification units.

A number of experimental tests were carried out to determine the performance of the test cells. These tests monitored the performance of the test cell under no-load and loaded conditions. The tests were done at 25 °C and 35 °C at a pressure of 0.5 bar and varying hydrogen and oxygen volume flow rates.

The no-load test showed that the MEA's performed best at high reactant flow rates of 95 ml/min for hydrogen and 38 ml/min for oxygen. MEA 1, 2, 3, and 4 achieved an open circuit voltage (OVC) of 0.936, 0.855, 0.486 and 0.34 V respectively. The maximum current density achieved for the MEAs were 0.3816, 0.284, $15x10^{-6}$, and $50x10^{-6}$ A/cm^2.

Under loaded conditions the maximum power densities achieved at 25 °C for MEA's 1, 2, 3, and 4 were 0.05, 0.038, $2.3x10^{-6}$, $1.99x10^{-6}$ W/cm^2 respectively. Increasing the temperature by 10°C for MEA 1, 2, 3, 4 resulted in a 16.6, 22.1, 1.79, 10.47 % increase in the maximum power density.

It was found that increasing platinum loading, flow rates, and temperature improved the fuel cell performance. It was also found that the catalytic, stability and adsorption characteristics of silver did not improve when combining it with iridium (Ir) and ruthenium oxide (RuOx) which resulted in low current generation. The low maximum power density thus achieved at a reduced cost is not feasible. Thus further investigation into improving the catalytic requirements of non Pt based catalyst material combinations is required to achieve results comparable to that of a Pt based PEMFC.

Table of Contents

Chapter 1 - Introduction and Overview

Chapter 2 – Literature Review

Chapter 3 - Design and Methodology

Chapter 4 - Measurements and Results

Chapter 5 – Conclusion and Recommendations

ANNEXURE A: Standard Thermodynamic Properties of Chemical Substances

List of Figures

List of Tables

Glossary of abbreviations and definitions

A

A - Amp

A.cm^{-2} - Amp per centimeter squared

Ag - Silver

atm - Atmosphere

Au - Gold

B, C

Cc - Cubic centimeters

cm^2 - Square centimetre

CNT - Carbon Nano Tubes

^{o}C - Degrees Celsius

D

DC - Direct Current

DMFC - Direct Methanol Fuel Cell

E

E - Electrolyser

e$^-$ - Electron

F

F - Faraday's constant

FC - Fuel cell

G

ΔG - Gibbs free energy

H

ΔH - Enthalpy value of reaction

HD-DB-15 - Electrical Connector

HIQ - Global Gas and Equipment Brand

HHV - Higher heating value

H$^+$ - Hydrogen proton

H$_2$ - Hydrogen gas molecule

H$_2$O - Water

I

I$_L$ - Limiting current

Ir - Iridium

IrO$_x$ - Iridium oxide

IrRuO$_x$ - Iridium ruthenium oxide

IV - Current Voltage

J

J - Joule

K

K - Kelvin

KΩ - Kilo - ohm

kJ - Kilojoule

kPa - Kilopascal

Kj.mol^{-1} - Kilojoule per mole

KOH - Potassium hydroxide

L

l/min - Litre per minute

l - Litres

M

M$_{H2}$ - Molecular weight of Hydrogen

M$_{O2}$ - Molecular weight of Oxygen

M$_{H20}$ - Molecular weight of Water

mA - Milliamps

mA.mm^{-2} - Milliamp per square millimetre

μA.cm^{-2} - microamp per square millimeter

MEA - Membrane electrode assembly

mm - Millimetre

min - Minute

ml.mim^{-1} - Millilitre per minute

mV - Millivolts

μm - Micrometer

μW.cm^{-2} - Microwatt per square centimeter

MCFC - Molten Carbonate Fuel Cell

MFC – Mass Flow controller

N

N$_{Hydrogen}$ - Molar flow rate of Hydrogen

N$_{Oxygen}$ - Molar flow rate of Oxygen

Ni - Nickel

Nm - nanometer

O

OCV - Open Circuit Voltage

F - Faraday's constant

P

Pt - Platinum

PEM - Polymer Electrolyte Membrane

PAFC - Phosphoric Acid Fuel Cell

PEMFC - Polymer Exchange Membrane Fuel Cell

PVC - Polyvinyl Chloride

RuOx - Ruthenium Oxide

PO_2 - Partial pressure of Oxygen

PH_2 - Partial pressure of Hydrogen

PH_20 - Partial pressure of Water

Q, R

R - Universal gas constant

RFC - Regenerative Fuel Cell

Ru - Ruthenium

S

ΔS - Entropy

Sccm - Standard Cubic Centimeter Per Minute

SEM - Scanning Electron Microscope

STP - Standard Temperature and Pressure

T

T - Absolute Temperature (K)

t - Time

U, V

V - Volts

V$_{H2}$ - Volume flow rate of Hydrogen

V$_{O2}$ - Volume flow rate of Oxygen

V$_{reversible}$ - Reversible Voltage

W, X, Y, Z

W - Watts

W.cm^{-2} - Watts per square centimeter

W.mm^{-2} - Watt per square millimeter

W.h - Watt hour

Chapter 1: Introduction

1.1 Background

Industrialisation and the advances in technological aids to enhance quality of life have placed enormous demands on energy sources (resultant load-shedding periods have been imposed in South Africa). The volatile political situation in the Middle East (major suppliers of oil) and the reality that oil resources are not unlimited has resulted in the practical need to explore alternate energy sources that are cost effective.

Historically, the first fuel cell was developed by Sir William Grove, with results published in the Philosophical magazine in February 1839 [1]. Fuel cells are electrochemical devices that convert chemical energy into electrical energy and heat. A typical polymer electrolyte PEMFC consists of Pt catalysed electrodes for the anode and cathode sides with a polymer electrolyte sandwiched in between. Fuels, usually hydrogen are supplied to the anode side of the cell where it is oxidised. The released electrons travel through an external circuit and the protons through the electrolyte. Oxygen is supplied to the cathode where it combines with the electrons and protons to produce electrical energy, heat and water as the by-products of this reaction [2].

Fuel cells have the potential to be a near zero-emission energy storage and supply system. This adds further attractiveness to researching various materials and material combinations in developing this technology due to the current global trend in reducing the amount of carbon emission generated by burning fossil fuels [3].

1.2 Statement of the problem

Commercialisation of PEMFC has been slow mainly due to the high cost of using Pt on the electrodes. Platinum electrodes are used due to the fast reaction kinetics which reduce energy losses and improves cell performance [4]. Advances have been made in the form of reducing the Pt loading from 25 mg/cm^2 to 0.05 mg/cm^2 without reducing its performance [5].

A study conducted by Howard on designing the optimal material combination for a PEMFC showed that a weight percentage combination of 60 % gold (Au) and 40 % Pt on the cathode electrode had a 66 % improvement on the maximum current density over the Pt coated cathode when tested at a temperature of 60 °C [6]. Although the performance of the cell

improved, the cost for enhancing the performance also increased by taking into consideration the current prices of Au (R471.41/gram) and Pt (R430.44/gram) as given on the 10 October 2015.

A non-platinum electro-catalyst for the PEMFC which comprised carbon supported tantalum oxide material for the cathode side of the PEMFC was developed by [7]. Their results in terms of electrical potential was comparable to that achieved using Pt but current density reached only as high as 9 % than that of Pt [7].

Further research is required in developing a low cost material combination which will exhibit the same or better catalytic activity of Pt on a PEMFC. This will then allow for the possibility of developing an affordable and independent power production technology for the future.

1.3 Aim

This study aims to investigate the effectiveness of using a non Pt material combination for the catalyst layer of a hydrogen fuel cell which will increase local knowledge in this technology. The materials to be investigated include depositing silver (Ag) particles onto the anode and a material combination of Ag, iridium (Ir), and ruthenium oxide (RuOx) onto the cathode. Ag was chosen due to its low cost when compared to Pt and reasonable catalytic activity, Ir was added to the cathode side to improve the catalytic activity and RuOx to improve the stability of the material combination against the formation of oxides on the catalyst surface.

1.4 Research methodology

The effectiveness of using non Pt material combination for the catalyst layer will be addressed as follows:

- Conduct an in-depth literature review on the operation and components of a fuel cell.
- Design and construct a standard test cell.
- Design experimental set-up.
- Develop a testing station.
- Develop operating procedure and parameter setting.
- Run experiments and gather results.
- Compare results.
- Conclude on results and experimental set-up.

- Make recommendations on enhancing performance.

1.5 Objectives

- To review work done on development and characterisation of PEMFC's.
- To design and construct test cell.
- To build a test station and develop an operation procedure.
- To evaluate the performance of Pt loaded catalyst and a non Pt loaded catalyst on a polarisation and power curve.
- To test the effects of varying hydrogen and oxygen flow rates.
- To test the effects of increasing Pt loading.
- To test the effects of a 10 ^{o}C temperature increase from an ambient temperature of 25 ^{o}C.

1.6 Delimitations

This study will be confined to the following:

- Testing the fuel cell up to 35 °C and a pressure of 0.5 bar.
- Purchasing, not manufacturing, the membrane electrode assembly from the USA. It will however involve manufacturing the fuel hardware and a humidification unit.
- Testing a single non Pt catalyst layer fuel cell.

1.7 Hypothesis

It is possible to produce an acceptable maximum power density between 0. 5 - 5 mW/cm^{-2} by using a fuel cell with low cost electrodes.

1.8 Assumptions

The non Pt loaded fuel cell will deliver an acceptable maximum power density at a lower cost than a Pt loaded fuel cell. The non Pt sample to be tested will form a basis for understanding its behaviour and associated problems, and allow for future research into fine tuning the electronic properties of non-precious metals to achieve comparable results at a reduced cost.

3

1.9 Scope

Three samples will be tested. Two comprised of different Pt concentration loading to ensure proper testing set-up and operating parameter settings to achieve published results. The other sample is a catalyst combination of Ag, Ir and RuOx on the cathode and Ag on the anode.

1.10 Ethics

The study will be conducted in a safe laboratory environment where all safety aspects and requirements will be adhered to.

1.11 Outline of study

The findings of this research work is presented in five main chapters

Chapter 2: This chapter reviews the relevant literature pertaining to fuel cells.

Chapter 3: This chapter focuses on the test cell design, test station design and operating procedure.

Chapter 4: This chapter evaluates the experimental results and forms the basis of discussion.

Chapter 5: This chapter contains conclusions based on the experiments conducted and recommendations for future research.

1.12 Summary

This chapter has presented the background of fuel cells, objectives and purpose of the study in evaluating the effectiveness of using a non Pt material in the fuel cell. The overview of the research was also presented.

Chapter 2 will give a literature review of the operation of a PEMFC, its components, maximum theoretical voltage, voltage losses and operating parameters that affect its performance.

Chapter 2: Literature Review

2.1 History of fuel cells

Fuel cell technology dates back to the 1800s but it was not until the 20th century that it was used successfully in space crafts to provide electricity and water. The idea that electricity can be produced by reversing the electrolysis of water was demonstrated by Sir William Groove in 1839 [8]. There was not much interest in the invention of fuel cells because of the unstable materials Groove used and there was no practical application for the fuel cell at that time. NASA realised the potential benefits of using fuel cells on manned space flights in the 1960s and invested in developing this technology [8]. Fuel cells are quiet, reliable and the production of electricity produces water as the by-product [8]. This was seen as an ideal supply of electrical energy and water for the astronauts. The added benefit was that the fuel cell could be used as an electrolyser to produce breathable oxygen, and hydrogen for fuel. Over the decades fuel cells have become more compact, powerful, stable, and applications have extended to the telecommunication, power generation and automobile industries [8].

2.2 Hydrogen as a fuel

Hydrogen is the simplest, lightest, and most abundant element in the universe. An atom of hydrogen consists of one proton and one electron. Hydrogen is high in energy density, and the generation of electricity using hydrogen fuels cells creates zero emissions [9]. Almost all practical fuel cells today use hydrogen or compounds containing hydrogen as fuel. As a result, there are effectively two main options for fuelling a fuel cell: by using hydrogen directly, or as a hydrogen carrier. A hydrogen carrier is a convenient chemical species which is used to convey hydrogen to a fuel cell. For example methane (CH_4) is a convenient hydrogen carrier because it is more readily available than hydrogen, if pure hydrogen is used directly it must be created first by steam reforming and then be stored before being used [9]. Hydrogen can also be made from various renewable resources such as bio mass, solar power, or wind power. The excess energy generated using ocean, solar, and wind power in particular could be used for the electrolysis of water to produce hydrogen and oxygen [9].

2.3 Types of fuel cells

There are different types of fuels cells that can use different fuels. The main differences between the fuel cells are the type of electrolyte used and operating temperature. The main types of fuel cells are discussed.

2.3.1 <u>Alkaline Fuel Cell (AFC)</u> - This type of fuel cell uses hydrogen and oxygen as the fuel, potassium hydroxide (KOH) as the electrolyte and a wide range of catalysts can be used e.g. Ag, nickel (Ni) and other noble metals. The temperature range of this fuel cell is dependent on the concentration of KOH used. Higher operating temperatures > 250 °C require a greater concentration of KOH about 85 weight percent KOH solutions are used. At lower operating temperatures < 120 °C, 35 to 50 weight percent KOH solution are used [10].

2.3.2 <u>Phosphoric Acid Fuel Cell (PAFC)</u> - This type of fuel cell uses impure hydrogen as the fuel and has an operating temperature range between 150 and 220 °C. Concentrated phosphoric acid is used for the electrolyte and platinum catalyst for the anode and cathode. The problem with this fuel cell is carbon monoxide poisoning which poisons the platinum catalyst [10].

2.3.3 <u>Polymer Electrolyte Membrane Fuel Cell</u> (PEMFC) - This type of fuel cell is supplied with hydrogen and oxygen, uses a polymer electrolyte membrane and has an operating temperature range between 20 and 100 °C. The polymer electrolyte membrane is a proton conductor and is made up of a perflourinated sulphonic acid polymer. The constraint with this membrane is that it needs to be sufficiently hydrated to be able to conduct protons. Platinum is the typical catalyst used in this fuel cell although current research is focused on developing alternative non - platinum catalyst to reduce the cost of a fuel cell [11].

2.3.4 <u>Molten Carbonate Fuel Cell (MCFC)</u> - This type of fuel cell has an operating temperature range between 150 - 220 °C and is composed of a molten carbonate salt mixture suspended in a porous, chemically inert matrix. The anode catalyst consists of porous sintered nickel and the cathode of nickel oxide. The various types of fuels MCFCs that have been operated on include hydrogen, carbon monoxide, natural gas, propane, marine diesel, and simulated coal gasification [11].

2.3.5 Regenerative Fuel Cell - This type of fuel cell is required to work as an electrolyser and a fuel cell. They are based on the PEMFC with specific focus on developing bi-functional electrodes that work well in both modes [12].

2.4 Cost of catalyst material

The cost of a PEMFC is dominated by the cost of the catalyst layer. Current international trading prices for the metals used as the catalyst in PEMFC are given below in Table 1.

Table 1: International prices of metals as given on the 12 0ctober 2015[13]

Metal	Cost(ZAR/gram)
Platinum	430.44
Silver	6.39
Iridium	231.95
Ruthenium	19.99

2.5 Operation of a fuel cell

A fuel cell is an electrochemical energy conversion device. It directly converts chemical energy into electrical energy. Hydrogen enters the fuel cell at the anode where it is adsorbed and stripped of its electrons.

Oxidation: Anode: $H_2 \rightarrow 2H^+ + 2e^- = 0$ V $\hspace{3cm}$ (1)

The protons move through the electrolyte and the electrons move through an external current to create electricity. Oxygen enters the fuel cell at the cathode where it combines with protons and electrons at the catalyst to form electricity and water [14].

Reduction: Cathode: $2H^+ + 2e^- + ½ O_2 \rightarrow H_2O = 1.229$ V $\hspace{2cm}$ (2)

Total Reaction: $½ O_2 + H_2 \rightarrow H_2O = 1.229$ V $\hspace{3cm}$ (3)
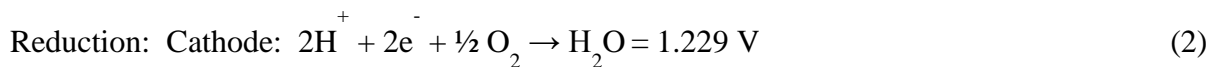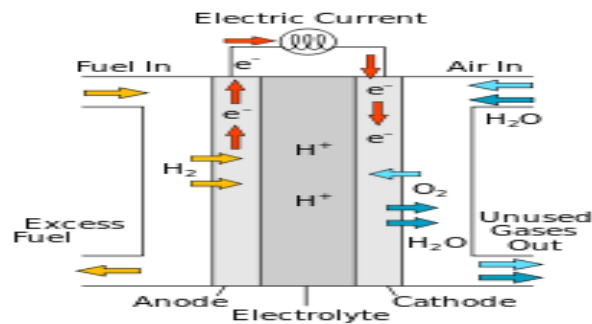
Figure 1: Operation of PEMFC [2]

2.6 The three phase reaction zone

A close look at the electrode in Figure 2 illustrates the reaction zone. The reaction zone is also referred to as the three phase boundary which consists of a catalyst, electron conductor (carbon support), and proton conductors (Polymer Electrolyte Membrane, or PEM). This is the area the reaction takes place. The reaction area can be increased by applying the catalyst particles onto a high surface area catalyst supports to obtain a higher amount of active reaction sites [15].
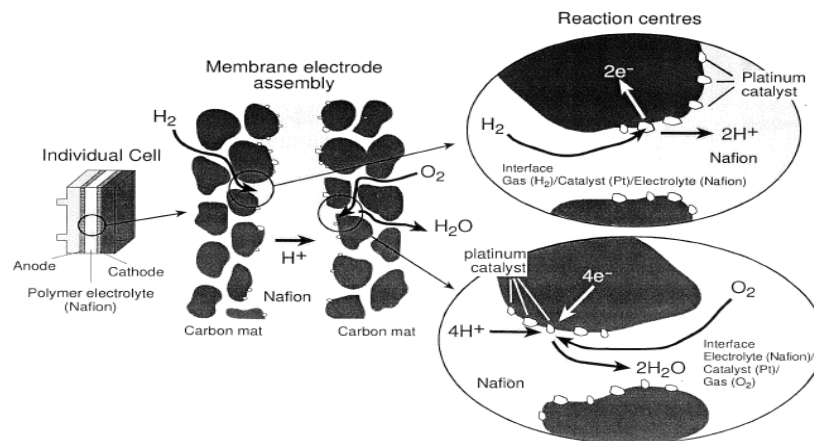
Figure 2: The three phase reaction zone [14]

Figure 2 shows that when hydrogen makes contact with the catalyst particles, the electrons released are conducted through the electrically conductive carbon support layer and the protons conducted through the polymer electrolyte for the anode reaction. The cathode reaction shows the entering electrons, protons and oxygen combining at the reaction sites to complete the reaction and form water H_2O.

8

2.7 Fuel cell components

The components that make up a PEMFC are shown in Figure 3 and will be discussed in this section, reason been that the focus of the current research is based on PEMFC. A PEMFC consists of a catalyst, gas diffusion layer, electrolyte, flow field plate, current collector, end plate, and gaskets.

A polymer electrolyte hydrogen fuel cell consists of a polymer electrolyte membrane on which catalyst particles supported on a carbon support are applied to on either side; this is called the membrane electrode assembly. A gas diffusion layer is placed on the catalytic active area to ensure good electrical contact between the flow field plate and active catalyst area. The flow field plates have machined gas channels to transport the gases to the reaction site. End plates are used to enclose the MEA and flow field plates. Gaskets are placed between the MEA's and flow field plates to prevent gas leaks and ensure proper sealing [16].
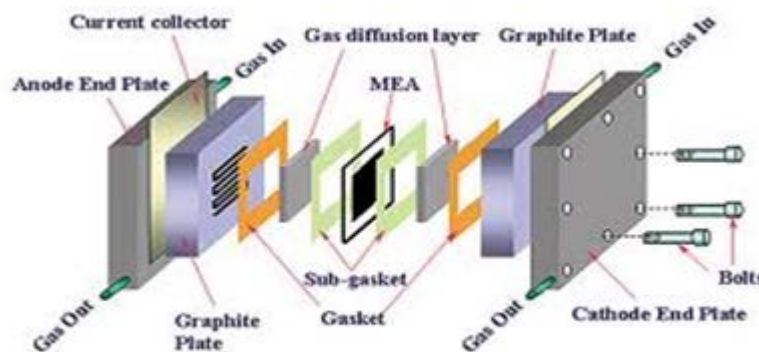
Figure 3: Fuel cell components and assembly [2]

2.7.1 Catalyst support

The function of the catalyst support layer is to provide a high surface area to dispense the catalyst particles. It is required to be stable and be electrically conductive. The catalysts are usually supported on carbon (Vulcan XC-72R) however, recent research has shown that the use of carbon nanotubes (CNT's) will provide a higher surface area, meaning more reaction zones and increase in power density [11][17].

2.7.2 Electro-catalyst

The function of the electro catalyst material is to accelerate the chemical reaction but not to be consumed in the process. A catalyst is a material that lowers the activation energy of a chemical reaction yielding a greater probability that a reaction will occur.

2.7.3 Requirements for a good electro-catalyst

2.7.3.1 Selectivity - the electro-catalyst must be able to minimise the production of undesirable products. Hydrogen peroxide (H_2O_2) is formed on the cathode when oxygen is adsorbed on the metal surface without the O=O bond being broken. This does not occur on the Pt surface as the O=O bond is broken when adsorbed, but for metals with weak binding to oxygen those undesired products can be highly damaging [18].

2.7.3.2 Durable – due to long hours (5000 hours/10 year) it is expected to perform.

2.7.3.3 Electronic-conductivity - must be electronically conductive to ensure good conduction of electrons to current collector plates or flow field plates. The electro-catalyst's electronic conductivity can be improved by applying it onto a conducting support to minimise resistance losses.

2.7.3.4 Electro-catalytic activity - the electro-catalyst needs to exhibit high catalytic activity. The exchange current density gives an indication of the catalytic activity of the material. The exchange current density represents the rate the reaction occurs at under equilibrium conditions - that is when the net current is zero i.e. open circuit [14]. The anode exchange current density in the H_2/O_2 fuel cell is several orders of magnitude larger that the cathode (10^{-4} vs 10^{-9} Acm^{-2}) at 25 °C and 1 atm when platinum is used [11].

Table 2: Exchange current density for the hydrogen evolution reaction at different electrode materials in aqueous H_2SO_4 [19]

Metal	I_o (A/cm^2)
Palladium, Pd	10^{-3}
Platinum, Pt	10^{-4}
Rhodium, Rh	10^{-4}
Iridium, Ir	10^{-4}
Gold, Au	10^{-6}
Silver, Ag	10^{-7}

Table 2 presents the exchange current densities for various metals from which the activation energy loss can be predicted (see section 2.8.1). Activation energy loss is the amount of energy lost from the equilibrium potential to start the reaction. An electro-catalyst with a high exchange current density has a high catalytic activity which reduces activation losses and increases the net current generated [14].

Most catalysts to date have been discovered by a trial and error approach. Considering the vast space of material combinations, however, it is quite likely that better catalysts are yet to be discovered [19].

2.7.3.5 Stability – the catalyst must not corrode in the operating environment of the fuel cell. Few metals are stable at the low pH and high electrode potential at the cathode of the fuel cell. Lack of kinetic activity due to the formation of oxide films on the metal surface shows poor stability of the metal catalyst. RuOx has high catalytic activity but is not stable under these conditions. Ir has a lower catalytic activity but greater stability according to Cheng and combining these metals will increase catalytic activity and have a stabilizing effect [20].

2.7.3.6 Adsorption characteristics- surface catalysis refers to the interaction of reactant on the surface of a catalytic particle. The Sabatier principle states that interaction must not be too weak or too strong it should be just right. If the interaction is weak the reactant would not be sufficiently adsorbed at the catalyst surface and a reaction will either not take place, or it will be slow. If the interaction is too strong the catalytic surface will quickly become blocked by the bound reactant, or the product will struggle to dissociate [18].

The Balandin volcano plot in Figure 4 shows the catalyst activity against the adsorption energy for metal hydrogen bonding. The plot shows a clear activity peak at which there are optimal bindings.
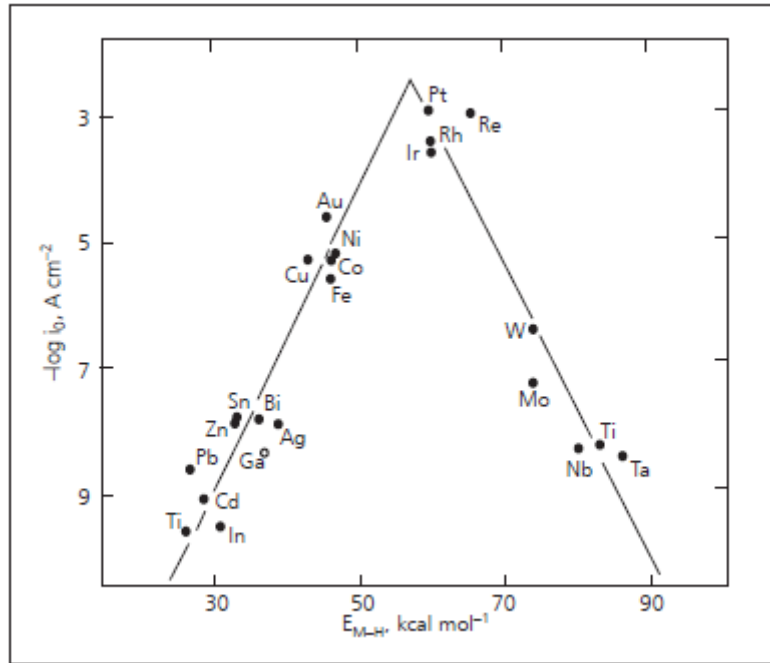
Figure 4: The logarithm of exchange current density (log i_0) for hydrogen evolution vs bonding adsorption strength of intermediate metal-hydrogen bond formed during the reaction itself [18]

Pt shows the highest catalytic activity for hydrogen oxidation reaction and is the target for fuel cell cost reduction. The extremely quick reaction results in a low activation energy loss which is neglible when compared to the cathode activation energy loss [11].
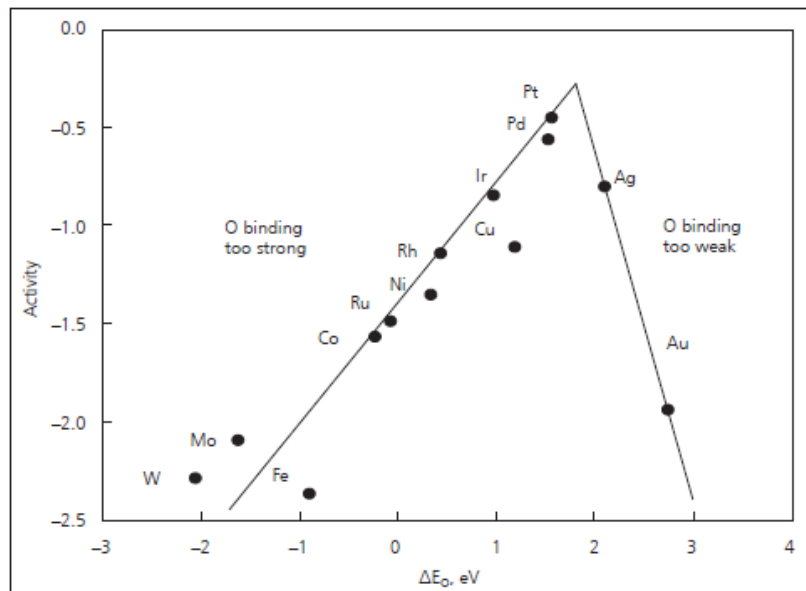
Figure 5: Oxygen reduction activity plotted as a function of the oxygen binding energy [17]

In Figure 5 Pt again shows the highest catalytic activity for the oxygen reduction reaction at the cathode but the oxygen bonding is still too strong by about 0.2V [17]. Strong bonding

causes the surface to become oxidised and unreactive which results in the reaction taking place slowly. Pt has the highest activity and shows optimal binding for both anode and cathode reactions. However the volcano plot shows that Pt does not sit at the peak. The ideal catalyst should have different electronic configurations according to the Sabatier principle, therefore research into fine tuning of the electronic configurations, primarily its d-orbital and electronic density of states of a substrate surface is required to achieve the ideal catalyst [18].

The area of this research focuses on using Ag for the anode and a combination of Ag, Ir and RuOx for the cathode catalyst taking into consideration the above mentioned factors. It is probable that catalytic activity and stability of Ag will increase by combining with Ir and RuOx.

2.7.4 Proton Exchange Membrane

The polymer electrolyte membrane (PEM) acts as a proton conductor. The H^+ ions are transported through the membrane structure when hydrated with water, and block movement of electrons through it. Nafion made by Du Pont is the PEM used in most commercially used fuel cells. The basic structure of Nafion is shown in Figure 6 [10].

$$(CF_2CF_2)_x \longrightarrow (CFCF_2)$$
$$|$$
$$O$$
$$|$$
$$(CF_2CF_2)_x \longrightarrow (CF_2)_m \longrightarrow SO_3^-H^+$$
$$|$$
$$CF_3$$
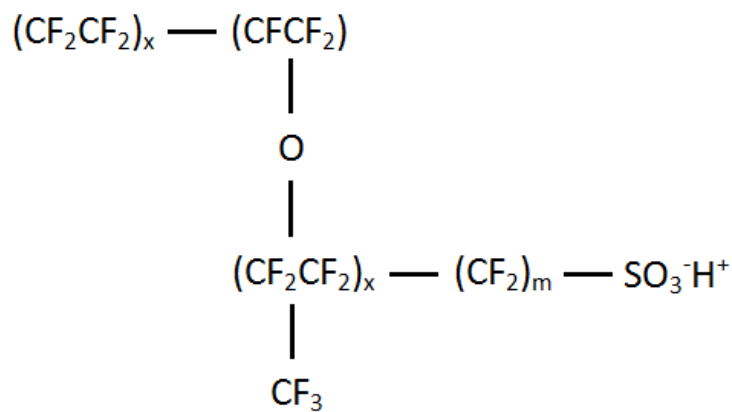
Figure 6: Nafion structure [10]

Nafion consists of carbon, fluorine and oxygen atoms with a SO_3H^+ at the end of the side chain. The side chain is ionically bonded so is actually an SO_3 molecule with H^+ ion. The H^+ ion is free to detach from the - SO_3H^+ and move from one SO_3 site to another thus conducting the proton through the membrane [21].

Nafion membranes exhibit the properties required for a membrane to be successful in achieving its function. The requirements for the membrane are as follows [21]:

13

- High proton conductivity

- Excellent chemical stability

- Acidic in nature

- High resistance to electron flow

- Does not allow hydrogen and oxygen molecules to diffuse though the membrane

The only drawback is that this existing state of the art membrane needs to be hydrated to facilitate the movement of protons through the membrane. Keeping the fuel cell sufficiently hydrated is crucial in maintaining optimum performance. Further research into developing a membrane which requires no hydration would reduce the complexity associated with the issue of water management.

Nafion is available commercially and come in a variety of different grades varying according to thickness as show in Table 3.

Table 3: Membrane types and thickness [22]

Membrane Type	Thickness(µm)
N-112	51
N-1135	89
N-115 & N-105	127
N-117	183
N-1110	254

The polymer electrolyte membrane is a transparent polymer film. The thickness of the membrane effects the distance the protons have to travel thus affecting the internal resistance, ohmic resistance and strength of the membrane. Nafion 115 is the membrane chosen as its reduced thickness allows for a balance between the internal resistance and strength of the membrane [22].

2.7.4.1 Water management

Proper water management is of utmost importance in achieving good fuel cell performance and durability. The two essential problems with water management are keeping the electrolyte hydrated and avoiding flooding of the electrodes. If the polymer electrolyte is not adequately hydrated proton conductivity decreases which results in an increase in cell

resistance and decrease in cell performance [23, 24]. Excess water causes flooding of the electrodes which prevent the reactant gases reaching the catalyst sites, increasing concentration over potentials and reducing cell performance. In order for the cell to be adequately hydrated the following factors need to be optimised to ensure the electrolyte is sufficiently hydrated: temperature of cell, humidification of reactants, reactant flow rates and cell design [23, 24].

Accumulation of water at the cathode is caused by the production of water at the cathode and electro osmotic drag. Electro osmotic drag refers to the movement of hydrogen protons which carry water molecules through the electrolyte from the anode to the cathode as shown in Figure 7. Accumulation of water at the anode is due to water back diffusion, which acts in the opposite direction of electro-osmotic drag and prevents the anode from drying out resulting in high ionic resistance [23, 24].
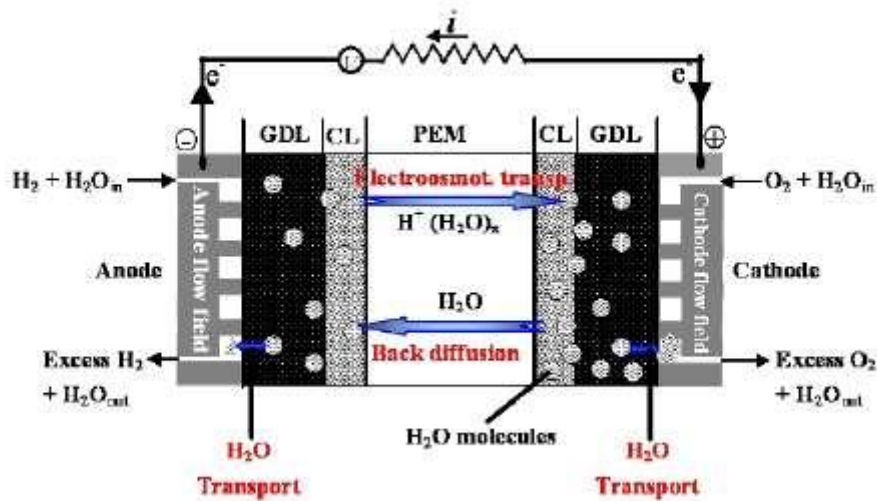
Figure 7: Electro-osmotic drag and back diffusion [23]

2.7.5 Gas diffusion layer

The function of the gas diffusion layer is to evenly distribute reactant to a catalyst layer and remove products from the catalyst layer to the flow field plate. It provides good electrical connection between the MEA and flow field plates. Carbon paper and carbon cloth are the most commonly used [11] [16].

2.7.6 Flow field plates

The functions of the flow field plates are to provide a pathway for the reactant gas to reach the reaction site, as well as electron conduction. Channels for the gases to travel to the catalyst layer are machined on to the inner surfaces of the plate's, one on the anode side and another on the cathode side.

Requirements for the flow field plates according to [25] are:

- High electrical conductivity
- Impermeable to gases
- Good thermal conductivity
- Light weight
- High corrosion resistance
- Easy to manufacture

Common materials used for the flow field plates are stainless steel 316, aluminium, graphite and composite materials [11].

2.7.7 Flow field design

The requirements of a good flow field design is to minimise the pressure drop between the inlet and outlet of the flow field plate and evenly distribute the reactants through the gas diffusion layer to the catalyst layer.

A. Pin type

The Pin type flow field design shown in Figure 8 consists of an array of equally spaced circular or cubical pins. The reactant gases flow through the grooves formed by the pins and cause a low pressure drop. The disadvantage of this arrangement is that the reactant gases tend to follow a path of least resistance which forms stagnant areas, leading to an uneven reactant distribution, and poor water removal and cell performance [26].
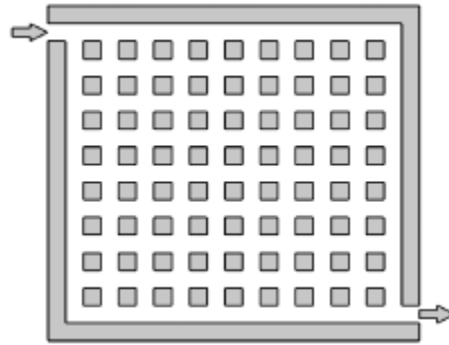
Figure 8: Pin type [22]

B. Single serpentine channel

In a single serpentine channel design shown in Figure 9, only one path for the reactant gas exists, from the inlet to the outlet, therefore no stagnant areas can be formed. This is an issue experienced by the pin type design. The pressure difference from the inlet to the outlet prevents the build-up of water in channels. The disadvantage of this design is that the reactants are depleted along the length of the channel therefore an adequate amount of gas must be supplied. Additionally, the relatively long continuous path causes a large pressure drop [27].
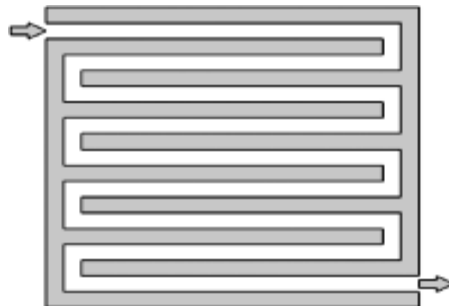
Figure 9: Single serpentine channel [22]

C. Several serpentine channels

In the several serpentine channel design shown in Figure 10, many different paths for the reactant gases to flow exist and offer a lower pressure loss than a single channel. This design also does not allow for the formation of stagnant areas. Disadvantages with this design are that of possible uneven gas flow distribution and water removal due to the many different paths that exist [27].

17

Mennola's research showed the preferred range of the channel width to be 1.14 -1.4 mm: 1.02 -2.04 mm for channel depth and 0.89 -1.4 mm for the land width [28].
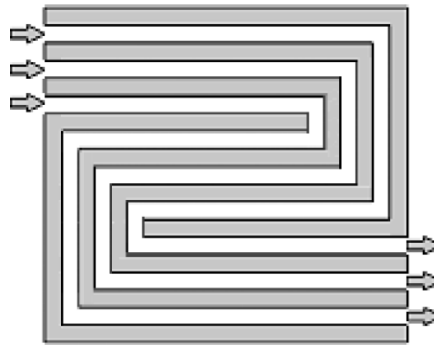
Figure 10: Several serpentine channels [22]

2.7.8 End plates

End plates are needed to hold the flow field plate and the membrane electrode assembly (MEA) together. The end plates are required to be stable over a required temperature range: to cost less, be vibration and shock resistant, mechanically stable, and have a high compressive strength. They also need to be easily machinable in order to provide connection points for the reactant gases. Commonly used materials for the end plates are [11]:

- Graphite
- Stainless steel
- Aluminium
- Titanium
- Nickel
- PVC
- Various other polymers

2.7.9 Sealing

Sealing and gaskets are required between the end plates and flow field plate to prevent gas leaking. Materials used for gaskets include silicone rubber, Teflon, and Teflon coated glass fibre thread plus adhesive [11] [29].

2.8 Chemical thermodynamics

Fuel cells are electrochemical energy converters that convert chemical energy of fuel directly into electrical energy. The main process of the fuel cell reactions which were described earlier is the same as the combustion of hydrogen reaction. The maximum amount of thermal energy that may be extracted from the combustion of hydrogen is determined by its higher heating value or enthalpy which is 286 kJ/mol at standard temperature and pressure (STP). The portion of hydrogen's higher value that can be converted to electricity in a fuel cell is called the Gibbs free energy and is equivalent to 237.34 kJ /mol [10]. This is the maximum energy input into the hydrogen fuel cell. The remaining 46.68 kJ /mol that is converted into heat is the entropy of the chemical reaction [10]. The theoretical energy required for the reaction to proceed can be expressed as follows:

$$\Delta G = \Delta H - T\Delta S \tag{4}$$

Where:

ΔG = Change in Gibbs free energy

ΔH = Enthalpy change of reaction

ΔS = Entropy change

T = Temperature in Kelvin

The maximum theoretical voltage of a cell is referred to as the reversible voltage ($V_{reversible}$) which can be obtained using Gibbs free energy. The reversible voltage for a hydrogen reaction that produces 2 electrons per molecule is shown below [14]:

$$V_{reversible} = \left(\frac{-\Delta G}{2F}\right) \tag{5}$$

$$V_{reversible} = \frac{-(237200)}{2(96485)} \tag{6}$$

$$V_{reversible} = 1.229 \text{ V} \tag{7}$$

Where :

$V_{reversible}$ = reversible voltage of a hydrogen fuel cell at standard temperature.

ΔG = change in Gibbs free energy of formation per mole.

F= Faradays constant (96485, 3 C.mol^{-1})

The reversible potential of the cell is affected by changes in temperature and pressure. Increasing the cell temperature reduces the theoretical potential as the amount of Gibbs free energy decreases as shown in Table 4.

Table 4: Change of enthalpy, Gibbs free energy and entropy of hydrogen/oxygen fuel cell reaction with temperature and resulting theoretical potential [5]

T(K)	ΔH	ΔG	ΔS	$V_{reversible}$ (V)
298.15	-286.02	-237.34	-0.16328	1.230
333.15	-284.85	-231.63	-0.15975	1.200
353.15	-284.18	-228.42	-0.15791	1.184
373.15	-283.52	-225.24	-0.15617	1.167

However increasing pressure increases the reactant partial pressures which improve the fuel cell theoretical potential. The cell potential as a function of temperature and pressure is given below [14]:

$$V_{reversible\ (T,\ P)} = \frac{\Delta H}{nF} - \frac{T\Delta S}{nF} + \frac{RT}{nF}\ln\frac{PH2\ PO2}{PH2O} \tag{8}$$

ΔH = Enthalpy change of reaction

n = Number of electrons

F = Faraday's constant = 96400 C/mol

ΔS = Entropy change

R = Gas constant = 8.314 J/mol*K

T = Temperature in Kelvin = 298 K at 25°C

PH_2 = Partial pressure of Hydrogen

PO_2 = Partial pressure of Oxygen

PH_2O = Partial pressure of H_2O

Equation (8) also shows that high concentration of reactants improves cell potential and if reactant are diluted it reduces cell potential. This can be seen in the case when air is used which has a partial pressure of 0.21 as a result of only 21 % oxygen in air i.e. partial pressure is proportional to concentration [10].

2.9 Over potentials

Losses of voltage below open circuit voltage are usually called over potentials and are shown in Figure 11. Those losses can be represented on an IV curve called a polarization curve which illustrates the overall performance of a fuel cell.
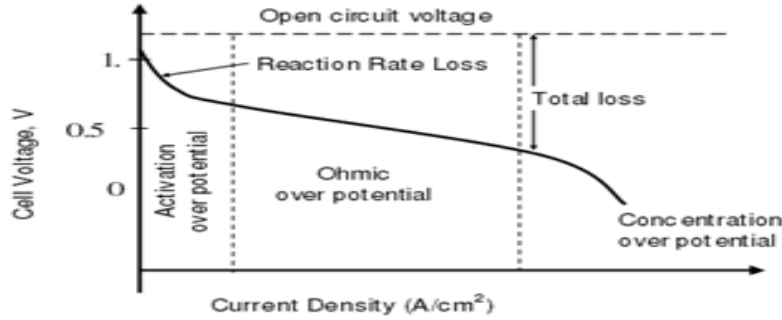
Figure 11: Polarization Curve [22]

The three main regions depicted above correspond to the three primary regions of over potentials in the polarisation curve:

1. Activation over potential
2. Ohmic over potential
3. Concentration over potential

$$V_{irreversible} = V_{activation} + V_{ohmic} + V_{concentration} \tag{9}$$

2.9.1 Activation over potential

Activation over potential refers to the amount of voltage difference from equilibrium needed to start the electro chemical reaction. The sharp drops in voltage at low current densities (1 to 100 mA/cm^2) are due to activation over potential. Activation over potentials occur at both the anode and the cathode, however there is a higher activation over potential at the cathode due to the sluggish oxygen reduction reaction, which implies that the reaction at the cathode is much slower than the reaction at the anode [30].

The activation losses can be expressed simply as the Tafel equation

$$\Delta V_{activation} = a + b \ln(i) \tag{10}$$

Where $a = \frac{RT}{aF} \ln(i_0)$ and $b = -\frac{RT}{aF}$

21

The anode and cathode activation losses can be calculated using equation below:

$$\Delta V_{activation} = \Delta V_{activation,\ anode} + \Delta V_{activation,\ cathode} \tag{11}$$

$$\Delta V_{activation} = \frac{RT}{anF}\ln\left(\frac{i}{io,anode}\right) + \frac{RT}{anF}\ln\left(\frac{i}{io,cathode}\right) \tag{12}$$

Where:

$\Delta V_{activation}$ = Activation energy losses (kJ/mol)

n = number of electrons

F = Faraday's constant = 96400 C/mol

a = charge transfer coefficient

i = operating current density (mA/cm^2)

$i_{0,\ anode}$ = exchange current density at the anode (mA/cm^2)

$i_{0,\ cathode}$ = exchange current density at the anode (mA/cm^2)

R = gas constant = 8.314 J/mol*K

T = temperature in Kelvin = 298 K at 25 ^{o}C

Equation (12) above shows that by increasing the exchange current density the electrodes become more active, which reduces the amount of activation energy required to start the reactions described earlier and also increases the net output current [14].

2.9.2 Ohmic over potential

Ohmic losses occur at intermediate current densities (100 to 500 mA/cm^2) and is represented by the straight portion on Figure 11 following the activation over potential region. Loss in voltage in this region is due to the resistance to the flow of electrons through the electrically conductive fuel cell components (R_{elec}) and to the flow of ions through the membrane (R_{Ionic}) [6].

$$V_{ohmic} = iR_{Ohmic} = I\ (R_{elec} + R_{Ionic}) \tag{13}$$

The electrical contact resistance is constant with respect to current and temperature. The ionic resistance is dependent on the water concentration and temperature of the membrane [31].

2.9.3 Concentration Over potential

Concentration losses occur at high current densities ($i > 500$ mA/cm^2) following the ohmic overpotential region. The fast drops in voltage are due to the depletion of reactants at high

current densities which causes rapid voltage loss. The current density at which the reactant concentration reaches zero at the catalyst surface is limiting current (I_L). Limiting current density only has an effect at high current densities. Operating the fuel cell at high current densities will not make sense as the maximum power can be reached at lower current density and higher potential. Generally fuel cells are operated at intermediate current densities [14]. The concentration losses are written as:

$$\Delta V_{concentration} = \left(\frac{RT}{anF}\right)\frac{IL}{IL-i} \tag{14}$$

Combing the above mentioned over potentials an expression for the operating voltage can be expressed in the following manner:

$$V_{cell} = V_{reversible} - (V_{activation} + V_{ohmic} + V_{concentration}) \tag{15}$$

A PEMFC using a platinum electro-catalyst operating voltage at 25 °C and 1atm with an operating current density of 200 mA/cm^2 can be calculated as follows using the parameters assumed below:

$a = 1$

$i_{0, anode} = 1 \times 10^{-4}$ Acm^{-2} (assuming a smooth surface)

$i_{0, cathode} = 1 \times 10^{-9}$ Acm^{-2} (assuming a smooth surface)

$R_{Ohmic} = 0.2$ Ωcm^2

$$V_{cell} = \frac{\Delta H}{nF} - \frac{T\Delta S}{nF} + \frac{RT}{nF}\ln\frac{PH2\,PO2}{PH2O} - \left(\frac{RT}{anF}\ln\left(\frac{i}{io,anode}\right) + \frac{RT}{anF}\ln\left(\frac{i}{io,cathode}\right)\right) - iR_{Ohmic}$$

$V_{cell} = 1.23 - [(8.314)\,(298)/\,(1)\,(96485)\,\ln\,(200 \times 10^{-3})/\,(1 \times 10^{-4}) +$

$\qquad (8.314)\,(298)/\,(1)\,(96485)\,\ln\,(200 \times 10^{-3})/\,(1 \times 10^{-9})] - (200 \times 10^{-3})\,(0.15)$

$V_{cell} = 0.5741$ V

2.10 Operating pressure

Reactant gases are supplied from a pressurised tank and controlled by pressure regulators. Operating the fuel cell at pressures higher then atmospheric pressure results in a higher cell potential as described by equation (8). [32, 33] investigated the effects of increasing pressures which is shown below.
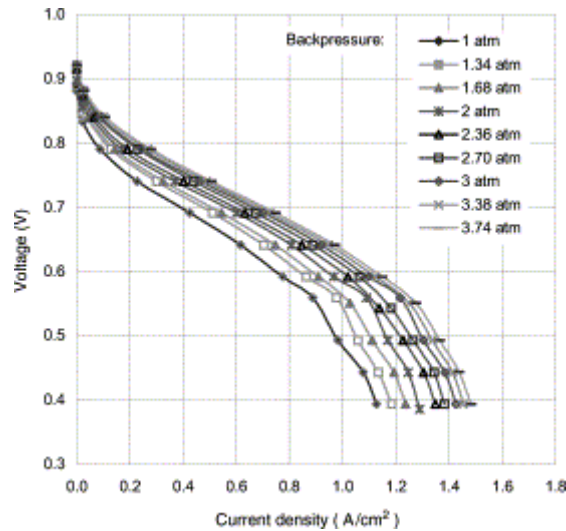
Figure 12: Effect of pressure [32]

It can be seen that increasing pressure positively shifts the polarization curve. Increasing pressure increases the reactant partial pressure and causes the equilibrium potential to increase. In terms of reaction kinetics, increasing pressure increases the reaction kinetics and exchange current density which lowers the activation over potential [32, 33].

2.11 Operating temperature

Polymer electrolyte fuel cell has an optimal temperature range that it can operate at (0-100°C). Increasing operating temperature can be achieved by heating the cell using heating pads or by following the US single cell test protocol [34].

The effects of temperature were investigated by [32], their results are shown in Figure 13.
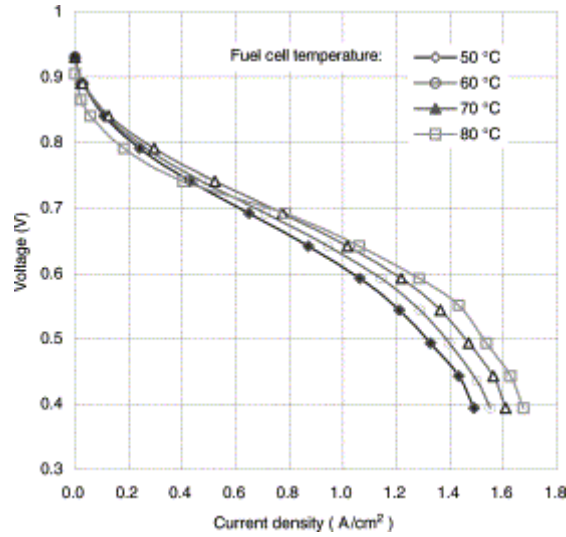
Figure 13: Effect of temperature [32]

Figure 13 shows that increasing temperature results in higher cell potential for a wide range of current densities. Increasing temperature improves the reaction kinetics and exchange current density which reduces the activation over potential [32, 33].

2.12 Reactant flow rate

Flow rates of the reactants can be controlled by mass flow controllers. The reactants must be supplied at a faster rate than which it is consumed. For pure hydrogen the required stoichiometry is 1.2 and for pure oxygen between 1.2 and 1.5 [11]. The rate at which the reactants are consumed and product formed can be determined by the following equations.

Mass flow rate of the reactants in consumptions (g s^{-1}) are:

$$m_{H2} = \left(\frac{i}{2F}\right)M_{H2} \tag{16}$$

$$m_{O2} = \left(\frac{i}{4F}\right)M_{O2} \tag{17}$$

$$m_{H2O} = \left(\frac{i}{2F}\right)M_{H2O} \tag{18}$$

Where:

M_{H2} = molecular weight of hydrogen

M_{O2} = molecular weight of oxygen

M_{H2O} = molecular weight of water

F = Faradays constant = = 96400 C/mol

i = current (A)

25

The volumetric flow rates of reactant consumption (standard litres per minute) are:

$$V_{H2} = 23.65 \times 60\left(\frac{i}{2F}\right) \tag{19}$$

$$V_{O2} = 23.65 \times 60\left(\frac{i}{4F}\right) \tag{20}$$

Higher flow rates improve fuel cell performance as it helps remove product water and keeps reactant concentration high at the reaction sites [14].

Volume flow rate calculation of reactants:

Molar flow rate of hydrogen and oxygen required for 1A and 1 cell.

$N_{hydrogen} = (I / 2F) = (1 / 2 \times 96485) = 5.182 \times 10^{-6}$ mol/s
$N_{oxygen} = (N_{hydrogen} / 2) = 2.591 \times 10^{-6}$ mol/s

Volume flow rate of hydrogen and oxygen required for 1A and 1 cell.

$V_{hydrogen} = 23.65 \times 60 \times 5.182 \times 10^{-6} = 7.35 \times 10^{-3}$ l/min
$V_{oxygen} = (V_{hydrogen} / 2) = 3.68 \times 10^{-3}$ l/min

Volume flow rate of hydrogen and oxygen required for the MEA's with an active area of $9cm^2$ in this research given below.

$V_{hydrogen} = 9(7.35 \times 10^{-3}) = 6.612 \times 10^{-2}$ l/min = 66.15 ml/min
$V_{oxygen} = (V_{hydrogen} / 2) = 33.075$ ml/min

2.13 Fuel cell efficiency

The fuel cell efficiency is the ratio between the actual operating voltage and hydrogen higher heating value or lower heating value [11].

Fuel cell efficiency using hydrogen higher heating value:

$$N_{fc} = \frac{V}{1.482} \tag{21}$$

Therefore the maximum theoretical efficiency at 25 °C and 1atm:

$$N_{fc} = \frac{1.229}{1.482} = 0.83 \tag{22}$$

Efficiency at the max power point:

$$N_{fc} = \frac{Vmp}{1.482} \tag{23}$$

A fuel cell operating at a maximum power of 0.5 V and 0.8 A/cm^2 results in an efficiency of 0.34. The same power can be achieved by connecting two cells in series and operating with a lower current density of 0.26 A/cm^2 at 0.77 V thus using less fuel, which will result in a higher efficiency but at twice the price [10].

2.14 Summary

This chapter discussed the important aspects pertaining to a PEMFC. The different component designs and materials that make up the PEMFC were identified. The components included a polymer electrolyte membrane, electro-catalyst, catalyst support, gas diffusion layer, flow field plates and end plates. The operation of PEMFC, its maximum theoretical voltage ($V_{reversible}$) and voltage losses at different current densities where explained. The operating parameters that effect the performance of the PEMFC were given. A sample calculation for the reversible voltage, voltage efficiency and volume flow rates of the reactant gases were provided. In chapter 3, the PEMFC design, assembly, experimental setup and testing methods will be discussed.

Chapter 3: Design and Methodology

This chapter focus is on the practical design, construction and assembly of a single PEMFC. The design and setup of the experimental test station to characterise the PEMFC are shown together with the testing methods applied.

The aim of the investigation was to:

- To build a test cell.
- To build a test station and develop an operation procedure.
- To test the effects of varying H_2 and O_2 flow rates.
- To test the effects of increasing Pt loading.
- To test the effects of a 10 ^oC operating temperature increase.
- To evaluate the performance of Pt loaded catalyst and a non Pt loaded catalyst.
- Compare cost versus power density of Pt and non Pt catalyst.

3.1 Test cell

The test cell components and specifications are detailed in Table 5.

3.1.1 Membrane Electrode Assembly (MEA)

The three MEA's tested in this study were purchased from FuelCelletc in the USA. The type of catalyst material, catalyst loading, electrolyte, gas diffusion layer and active area are presented in Table 5. An image of the MEA is shown in Figure 14.

Table 5: The membrane electrode assembly specifications

MEA	Catalyst Material on Anode	Catalyst Material on Cathode	Catalyst loading on Anode	Catalyst loading on Cathode	Electrolyte	Gas Diffusion Material	Active Area
1	Pt	Pt	$0.1mg/cm^2$	$0.1mg/cm^2$	Nafion 115	Carbon Cloth	$9\ cm^2$
2	Pt	Pt	$0.3mg/cm^2$	$0.3mg/cm^2$	Nafion 115	Carbon Cloth	$9\ cm^2$
3	Ag	Ag + IrRuOx	$2mg/cm^2$	$1.5mg/cm^2$ + $1.5mg/cm^2$	Nafion 115	Carbon Cloth	$9\ cm^2$
4	Ag + IrRuOx	Ag	$1.5mg/cm^2$ + $1.5mg/cm^2$	$2mg/cm^2$	Nafion 115	Carbon Cloth	$9\ cm^2$
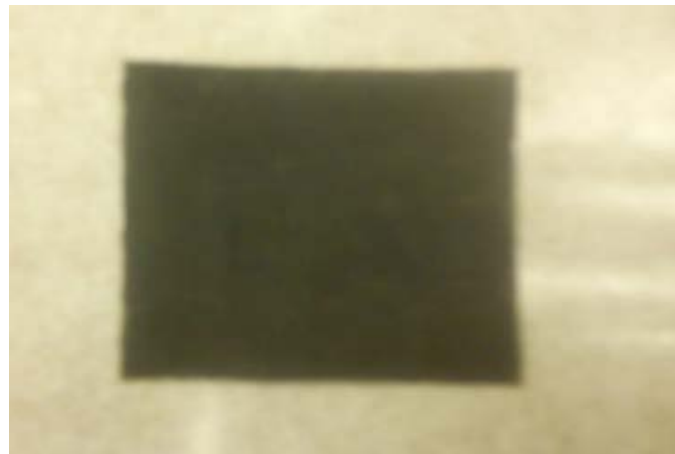
Figure 14: MEA purchased from the fuel cell store

3.1.2 Flow field plates

The flow field plates used to transport the hydrogen and oxygen gases to their reaction sites are made of aluminum with a 2 mm thickness. Aluminum was used as it was cost effective and exhibits the properties required for this application. The flow field design consisted of 23

circular holes with a 3 mm diameter. The dimension of the flow field design is shown in Figure 15. This flow design was chosen due to its simplicity and the low cost involved in developing the flow field design. The flow field design drawings are shown in Figure 15 and were done on Microsoft Visio.
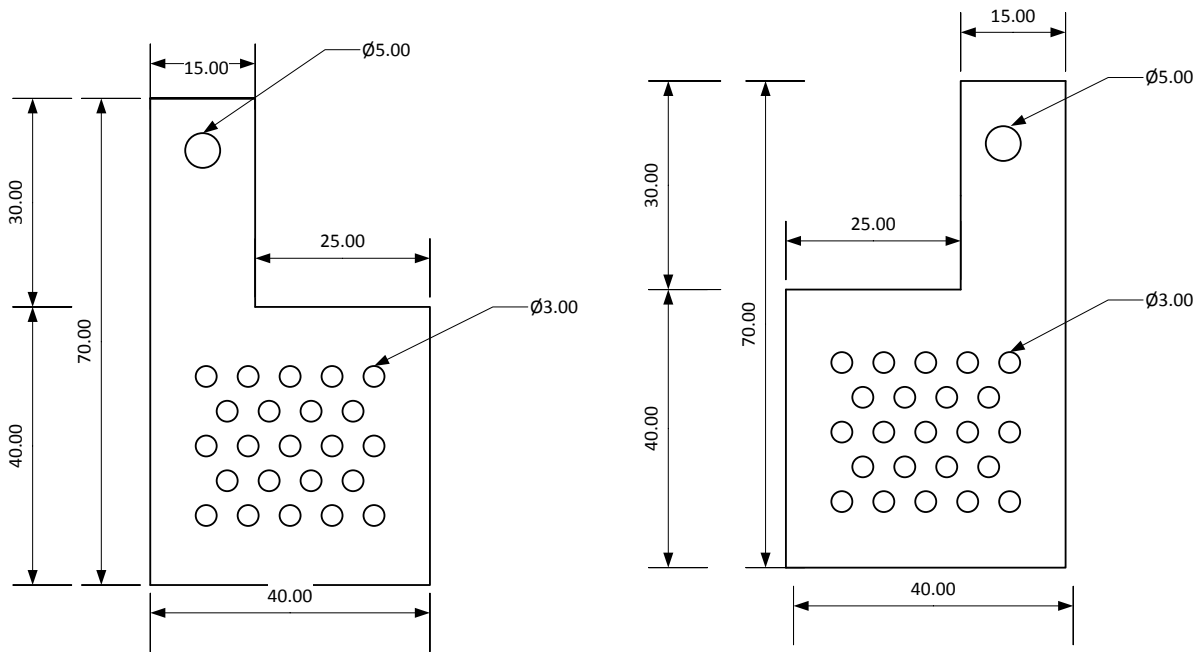
Figure 15: Flow field design

3.1.3 End plates

The material used to enclose the MEA and flow field plates were made from perspex to ensure the anode and cathode were visible. The dimensions of the end plates were 65 mm x 65 mm x 10 mm. The end plates provided four connection points with a diameter of 4 mm for the bolts to hold the fuel cell together. Two more holes on each end plate of diameter 8 mm were drilled and threaded to provide connection points for the reactant gases. The drawing for the perspex end plate is shown in Figure 16.
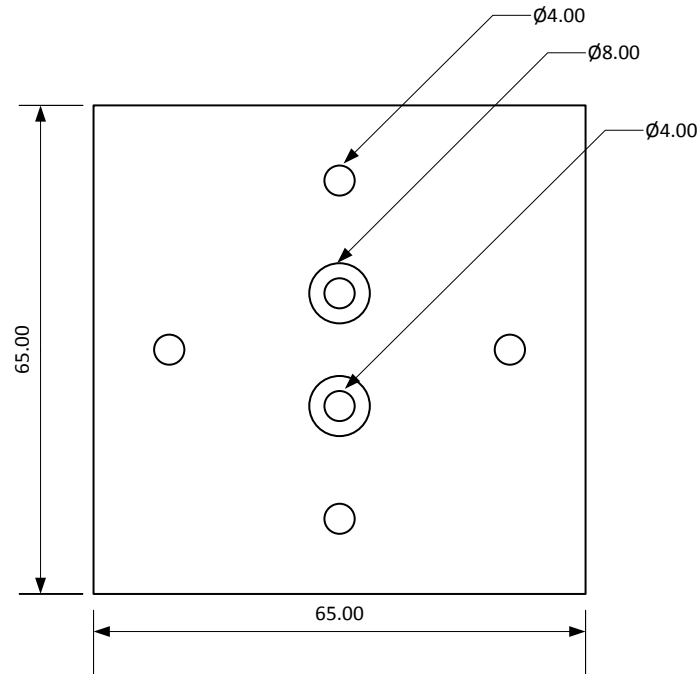
Figure 16: Perspex end plates

3.1.4 MEA pre-treatment

In order to improve the membrane proton conductivity and catalyst performance each MEA was soaked in di-ionised water for up to 100 hours before being assembled in the fuel cell [34-38].

3.1.5 Assembly of test cell

Each MEA was placed between two flow field plates with attached gas diffusion layers. A silicone gasket was placed on the inside face of the end plates to prevent gas leaking and separate the end plate from the flow field plate. The two end plates with attached silicone gaskets were then placed against the flow field plates to enclose the fuel cell. The MEA and flow field plates were now enclosed by the two end plates. Both end plates were held together with eight bolts with washers and nuts. The nuts were first hand tightened to ensure the end plates were aligned parallel to each other. The bolts were then tightened to a torque of 3 Nm.

3.2 Test station equipment

The equipment used for the test station is presented on pages 31 - 36.

31

3.2.1 Hydrogen generator

The PEAK scientific hydrogen generator was used to supply hydrogen to the cell. The generator uses de- ionised water and a PEM electrolyser to produce a continuous stream of high purity (99, 99 %) hydrogen gas. When the unit is initially started, the gas goes through a series of internal checks to ensure there are no leaks in the system after which the hydrogen downstream pressure can be automatically set before hydrogen delivery. PEAK scientific hydrogen generators are ideal for use in laboratories and high industrial environments, with hydrogen production capabilities of 100 cc/min – 300 cc/min [39]. The PEAK scientific generator is shown in Figure 17.
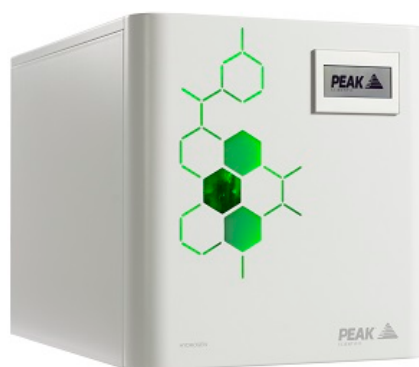
Figure 17: PEAK scientific hydrogen generator [39]

3.2.2 Humidification unit

The humidification units were manufactured using a perspex cylinder with 5 mm thickness, square perspex pieces, brass pipe fittings, and a brass non return valve. The height of the cylinder was 350 mm with an inner diameter of 90 mm. The dimensions of the square pieces used to enclose the cylinder were 110 mm x 110 mm x 4 mm. The square pieces were plastic welded to both ends of the cylinder. The humidifier was filled with 1.5 litres of de-ionised water so that the gasses could be bubbled through. The cylinder was pressure tested up to 4 bars to ensure no leaking. The brass non-return valve was inserted 25 mm from the bottom of the cylinder and the brass fitting was threaded on the top of the cylinder to provide a connection for the piping to the cell as shown in Figure 18.
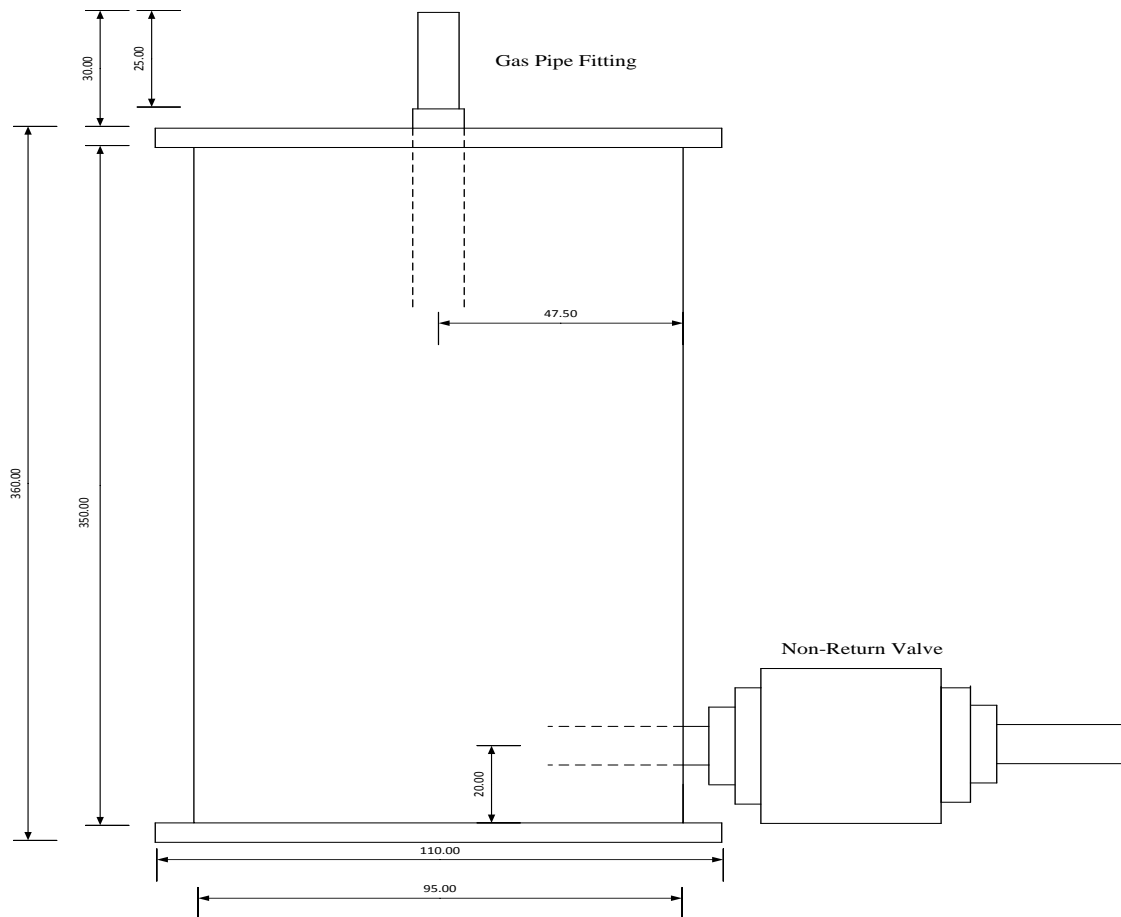
Figure 18: Humidification unit

3.2.3 Mass flow controller

The Sierra mass flow controllers shown in Figure 19 were used to measure the flow of hydrogen and oxygen during the experiment. Smart - Trak mass controllers allowed for accurate and repeatable mass flow measurement and control. The unit was powered from a 24 V DC, 500 mA regulated dc Siemens supply. The controller has many features such as the dial a gas feature which allows for the selection of gases to be measured and controlled without losing its accuracy [40]. The instruments have three control options:

1. Analogue Input/output operation with a HD –DB –15 connection
2. Digital operation with pilot module
3. Digital operation with RS -232 and Smart - Trak software

Upon start up, the pilot module will allow for a variety of parameter settings on the lower level that include [39]:

- Set point value

- Engineering units

- Gas type

- Valve operation (normal, closed, purge)

- Source of the set point signal (analogue or digital)

- Form of the output signal

- Full scale of the instrument

- Password

- Zero

- Span

The upper level of the pilot module displays information

- Mass flow rate

- Gas(10 options –pre-programmed)

- The engineering unit

- Current set point

- Valve operation

The specifications of the Sierra Smart - Trak 100 are as follows:

- Model 100L

- Range 0-10 standard cubic centimeters per min(sccm)

- Standard calibration ±1% of full scale at operating conditions

Figure 19: Mass flow controller [40]

3.2.4 Oxygen

Pure HiQ oxygen stored in a cylinder and purchased from Afrox was used.

3.2.5 Pressure regulator

Pressure regulators made by AMFLO was used to set the gas pressure released from the Hydrogen and Oxygen cylinder to 50 KPa.

3.2.6 Gas piping

Certified hydrogen and oxygen piping with a diameter of 8mm and 4mm flexible tubing was used.

3.2.7 24 V DC power supply

The Siemen's 24V DC power supply shown in Figure 20 was used to energize the each of the two Smart - Trak mass flow controllers.
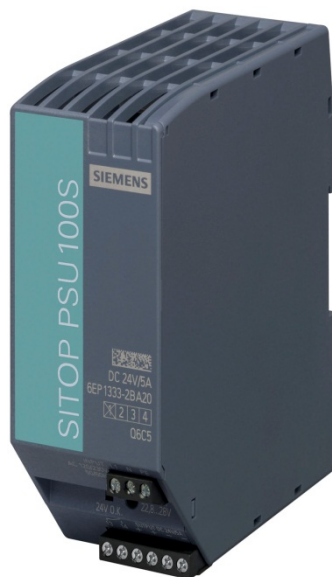
Figure 20: Siemens 24V dc supply

3.2.8 Current, voltage and temperature meters

Voltage and current measurements were taken with a Fluke 177 multi-meter shown in Figure 21. The Fluke 178 with a k-type thermocouple shown in Figure 22 was used to measure the temperature.

Figure 21: Fluke 177 multi-meter

Figure 22: Fluke 178 multi-meter

3.2.9 Variable resistive load

A variable resistor with a range of 0.1 Ω - 10 kΩ was used.

3.3 Experimental setup

The test station to characterise the test cell performance shown in Figure 23 and 24 was situated within a vacuum and with an extraction fan operating to ensure safety when working with hydrogen gas. Flashback arrestors were already installed on both oxygen and hydrogen cylinders as additional safety requirements in case of an explosion in either of the gas feed lines. Certified hydrogen and oxygen piping was used for connections from the pressure regulator to the mass flow controllers and humidification unit. The piping diameter was reduced to a 4 mm flexible pipe from the humidification unit to the test cell. The flexible

36

piping was then connected to the inlets of the test cell. The mass flow controllers were manually set using the pilot interface. The humidification units to humidify the reactant gases to the test cell had to be manufactured as commercially available units were not designed to withstand pressure above atmospheric. The unit has a capacity of 2 L which was filled with de-ionised water to a volume of 1.5 L, which allowed gases to be bubbled, through at high flow rates without water spilling out.

A variable resistor with operating range of 0.1 -0 KΩ was used as the load and varied to alter the load current and voltage. A heating plate with a temperature range 0 -200 °C was used to increase the cell temperature to the required value for testing. The results displayed on the multi-meters for current, voltage, and temperatures were manually recorded.
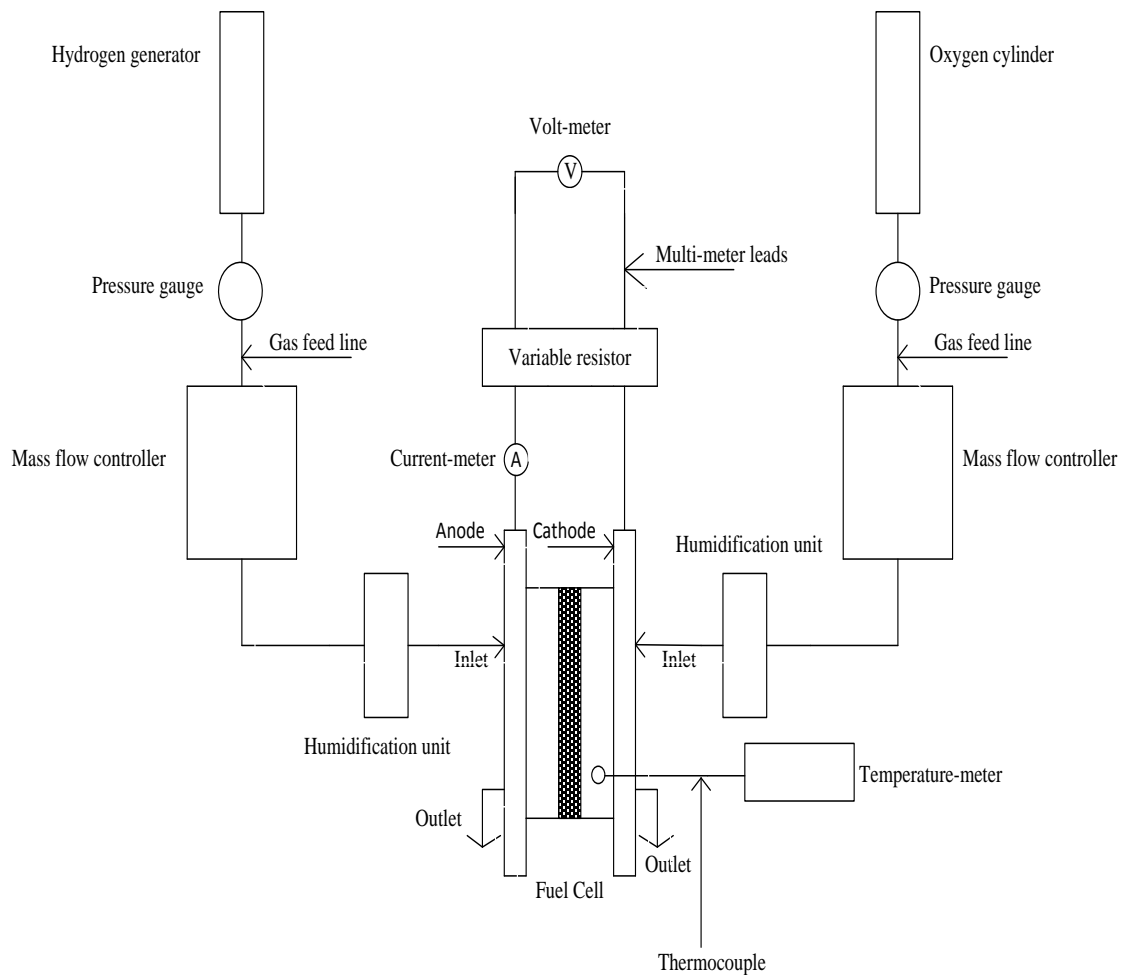
Figure 23: Schematic of experimental setup

Figure 24: Experimental set-up

3.4 MEA activation

Two operating procedures were developed: One for no - load, and the other for varying load conditions. Under no - load conditions the fuel cell (MEA 1, 2, 3, and 4) was run for 20 minutes before results were taken. Under varying load conditions, the fuel cell (MEA1, 2) was loaded for 1 hour (30 min at 500 mV and 30 min at 400 mV). MEA 3 and 4 was also run for 1 hour (30 min at 200 mV and 30 min at 300 mV) [34-38]. These voltages were selected as they are within the operational voltage range of the MEA's being investigated. The MEAs were then fully characterised by varying the load in steps of 0.1 Ω from 0.1-1 KΩ and results recorded to plot the polarisation curve. Two minute intervals were allowed before a set of readings were recorded. After this characterisation sequence the cycle was complete. This cycle was repeated twice to observe any improvement in performance. It was noted that when the cell was run immediately after the first cycle that there was a slight improvement in performance.

3.5 PEMFC tests

The test to characterise the performance of the three MEA's on a polarisation curve was conducted at a pressure of 0.5 bar at 25 °C and 35 °C using humidified hydrogen and oxygen. The hydrogen and oxygen flow rates required for 1 A were calculated using equations (19) and (20) from section 2.12 and were then increased stoichiometrically. The polarisation curve for each MEA was obtained by first measuring the OCV then gradually decreasing the potential to near limiting current densities. A waiting period of 2 minutes was allowed for the current density to settle between each step. A set of current density and potential values were

recorded and used as data points for the polarisation curve. The power curve was obtained by multiplying the current density by the cell potential.

3.5.1 Open circuit voltage test

Each MEA was run under conditions mentioned above. The hydrogen volume flow rate range was 19 – 95 ml/min and oxygen 7 – 38 ml/min. The oxygen volume flow rate was held constant at 7, 19, 38 ml/min while hydrogen volume flow rate was increased by 19 ml/min throughout its range. The experiment for the open circuit voltage of MEA 3 and 4 held the oxygen volume flow rate at 38 ml/min and hydrogen varied using the mass flow controllers..

3.5.2 Maximum current density test

Each MEA was run under conditions mentioned for the open circuit voltage test. It was noted that the multi-meter used had an internal resistance of 0.1 Ω.

3.5.3 Efficiency test

Current efficiency was obtained from the ratio of the current produced and the current that should be produced from the calculation. Voltage efficiency was obtained from the ratio of the cell voltage and the thermodynamic potential (hydrogen higher heating value). The overall efficiency is the product of the current and voltage efficiency.

3.6 Experimental procedure

- Switch on MFC and set required gas flow rates.
- Switch on hydrogen generator at set pressure to 0.5 bar.
- Open oxygen cylinder valve and set pressure to 0.5 bar.
- Run the cell for 20 minutes under open circuit condition.
- Connect variable resistor.
- Run cell under varying load setting and record voltage and current values.

3.7 Safety precautions

Since we were working with hydrogen which is a potentially explosive gas the following safety precautions were taken:

- Ensure extraction fan in lab was on.

- Ensure vacuum was placed over the cell during experimentation.
- Flashback arrestors on hydrogen and oxygen regulator which were already installed in the lab.

3.8 Summary

This chapter presented the test cell design, experimental setup, and testing methods. The individual component design, drawings, manufacturing, and assembly of the PEMFC were provided. The experimental setup included mass flow controllers, hydrogen and oxygen sources, pressure regulators, humidification unit and voltage, current and temperature meters. The humidification unit was manufactured and the drawing design presented. The operating parameter settings were given together with the testing specification for each experiment carried out. The safety precautions taken during the experiments were also outlined. In Chapter 4, the results obtained will be given and analysed.

Chapter 4: Results and discussion

This chapter tabulates and graphically shows the results obtained from the testing methods mentioned in Chapter 3. The analyses of each experiment carried out are presented.

4.1 Open circuit voltage

Table 6: MEA 1, varying hydrogen and oxygen flow rates with respective voltages

Hydrogen flow rate (ml/min)	Voltage at oxygen flow rate of 7 ml/min (V)	Voltage at oxygen flow rate 19 ml/min (V)	Voltage at oxygen flow rate 38 ml/min (V)
0	0	0	0
19	0.87	0.931	0.934
38	0.892	0.934	0.935
57	0.945	0.935	0.935
76	0.946	0.935	0.936
95	0.949	0.939	0.936
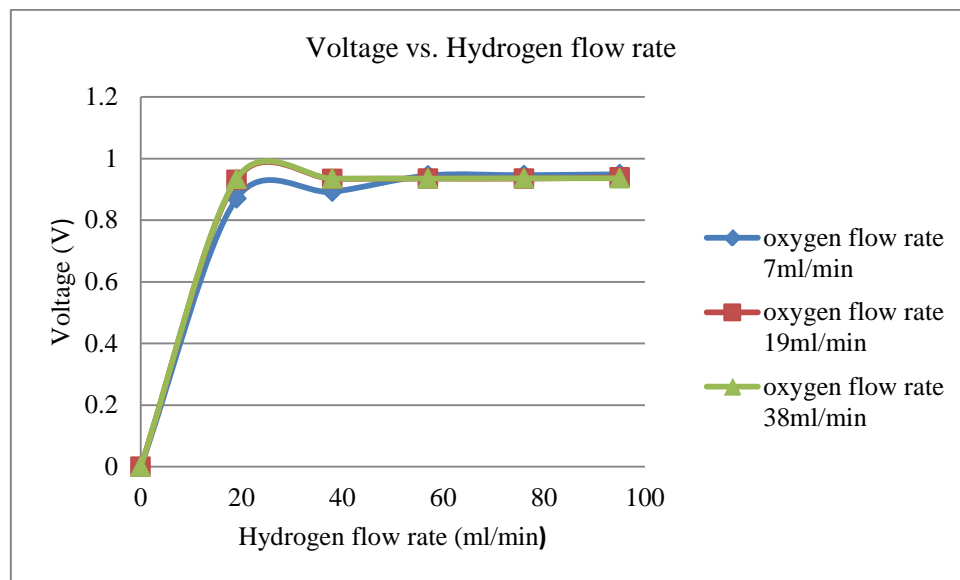
Figure 25: MEA 1, varying hydrogen and oxygen flow rates with respective voltages

Table 7: MEA 2, Varying hydrogen and oxygen flow rates with respective voltages

Hydrogen flow rate (ml/min)	Voltage at oxygen flow rate of 7 ml/min (V)	Voltage at oxygen flow rate 19 ml/min (V)	Voltage at oxygen flow rate 38 ml/min (V)
0	0	0	0
19	0.794	0.856	0.853
38	0.794	0.856	0.854
57	0.795	0.857	0.854
76	0.796	0.857	0.855
95	0.795	0.858	0.855
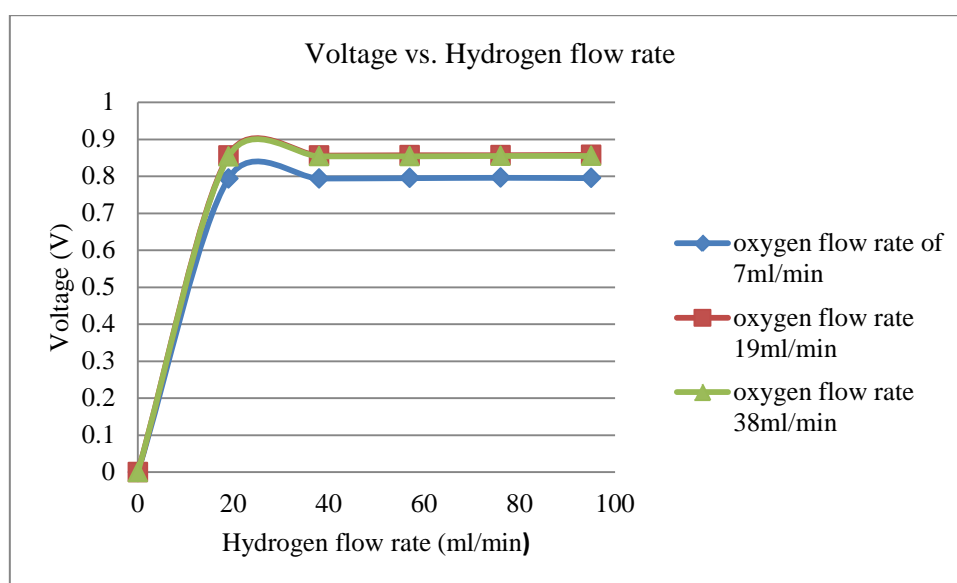
Figure 26: MEA 2, Varying hydrogen and oxygen flow rates with respective voltages

Table 8: MEA 1 vs. MEA 2, open circuit voltage, varying H_2, 7 ml/min O_2

Hydrogen flow rate (ml\min)	Oxygen flow rate (ml\min)	MEA1 (V)	MEA2 (V)
0	7	0	0
19	7	0.87	0.794
38	7	0.892	0.794
57	7	0.945	0.795
76	7	0.946	0.796
95	7	0.949	0.795
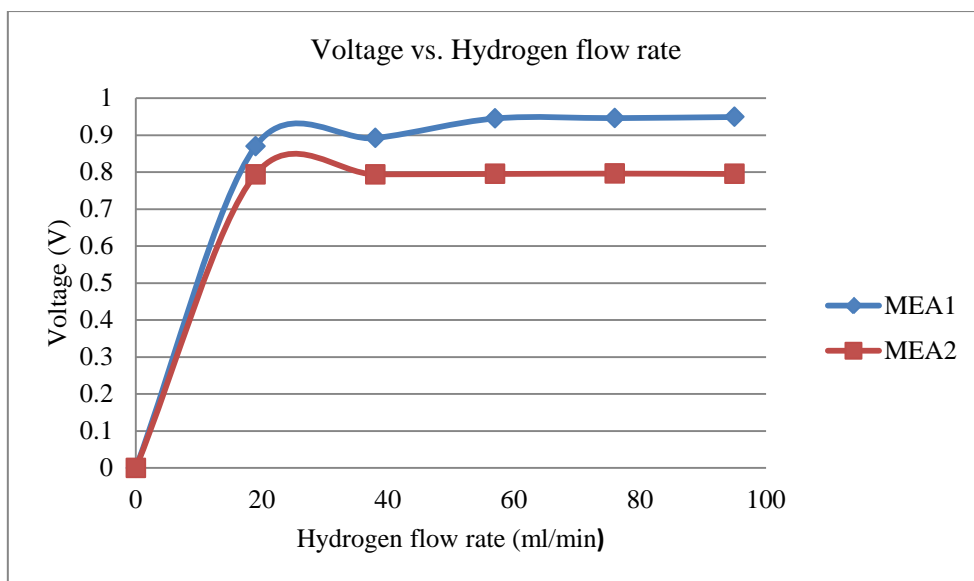
Figure 27: MEA 1 vs. MEA 2, open circuit voltage, varying H_2, 7 ml/min O_2

Table 9: MEA 1 vs. MEA 2 open circuit voltage, varying H_2, 19 ml/min O_2

Hydrogen flow rate (ml\min)	Oxygen flow rate (ml\min)	MEA1 (V)	MEA2 (V)
0	19	0	0
19	19	0.931	0.856
38	19	0.934	0.856
57	19	0.935	0.857
76	19	0.935	0.857
95	19	0.939	0.858
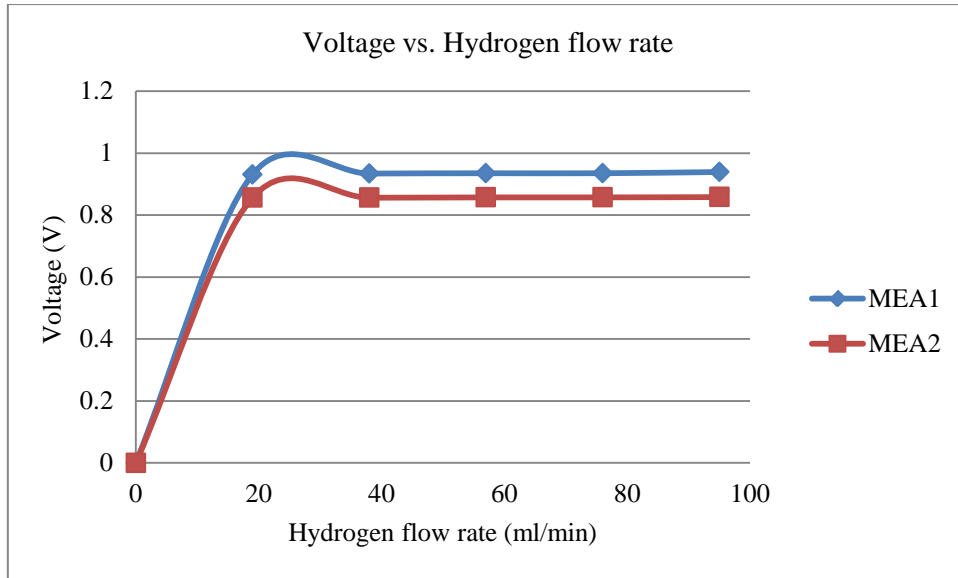
Figure 28: MEA 1 vs. MEA 2 open circuit voltage, varying H_2, 19 ml/min O_2

Table 10: MEA 1 vs. MEA 2 vs. MEA 3 vs. MEA 4, open circuit voltage, varying H_2, 38 ml/min O_2

Hydrogen flow rate (ml\min)	Oxygen flow rate (ml\min)	MEA1 (V)	MEA2 (V)	MEA3 (V)	MEA4 (V)
0	38	0	0	0	0
19	38	0.934	0.853	0.484	0.335
38	38	0.935	0.854	0.485	0.34
57	38	0.935	0.854	0.485	0.34
76	38	0.936	0.855	0.485	0.34
95	38	0.936	0.855	0.486	0.34
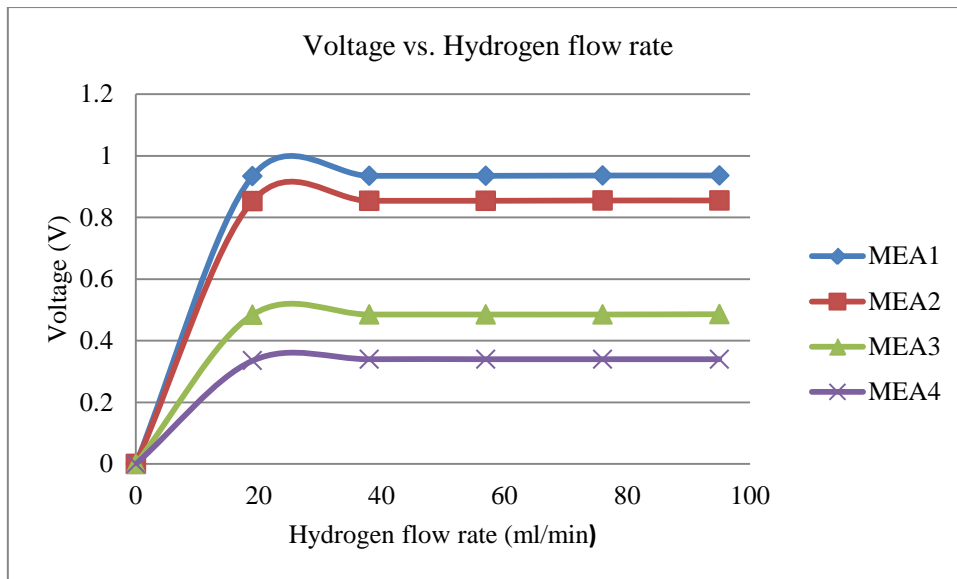
Figure 29: MEA 1 vs. MEA 2 vs. MEA 3 vs. MEA 4, open circuit voltage, varying H_2, 38 ml/min O_2

The effect of varying reactant flow rates for the MEAs tested are shown in Figures 25 - 29 and results tabulated in Tables 6-10. Oxygen flow rates were held constant at 7, 19, 38 ml/min while varying hydrogen flow rate at 19, 38, 57, 76, 95 ml/min. The voltages recorded and displayed were taken after a 20 minute time interval. The initial temperature was approximately 25 °C. The temperature measured from the current collector plate after 20 minutes was approximately 26.5 °C.

It was noted that the initial open circuit voltage was slightly higher than that recorded after 20 minutes. This was expected according to equation (5) as increasing temperature reduces the amount of Gibbs free energy, which causes the slight decrease in open circuit voltage.

The open circuit voltages of the MEAs improved slightly as the reactant flow rates were increased. However it was observed that not all the reactants were being utilized. The outlet for the reactants was placed in a water reservoir to confirm this. This suggests that fuel cells can be operated at reasonably higher flow rates to improve open circuit voltage performance, provided the exhaust reactants are recirculated into the cell so that the fuel utilization efficiency is improved.

The results obtained also shows that there is a small voltage difference between the maximum theoretical voltage (1. 23 V) and the best open circuit voltages measured for the MEA 1 and 2. The voltage difference between MEA 1 and 2 is due to the different catalyst loading for the

45

two MEAs. Lowering of the platinum loading appears to affect the open circuit voltage. This could be as a result of less active reaction sites for reactants to react with.

The larger voltage difference for MEA 3 and 4 was expected. The poor open circuit voltage of MEA 3 and 4 to the platinum loaded MEAs can be attributed to the use of a cheaper material with poor catalytic properties. The relatively poor catalytic properties of these materials adsorb reactants strongly, thus requiring more energy for the surface reaction to occur.

MEA 1, 2, 3, and 4 shows a deviation of 23.9 %, 30.5 %, 60.5 % and 72.4 % respectively. The general cause of the deviation of potential for the MEAs could be due to gas leaking within the cell or hydrogen permeation through the polymer electrolyte membrane, causing internal short circuit currents resulting in the added voltage deviation.

4.2 Current Density

Table 11: MEA 1, current density at varying reactant flow rates

Hydrogen flow rate (ml/min)	Current density at oxygen flow rate of 7ml/min (A/cm^2)	Current density at oxygen flow rate 19ml/min (A/cm^2)	Current density at oxygen flow rate 38ml/min (A/cm^2)
0	0	0	0
19	0.0237	0.1666	0.1555
38	0.0386	0.2988	0.3378
57	0.2111	0.3008	0.3787
76	0.2166	0.3105	0.3812
95	0.2222	0.3252	0.3816
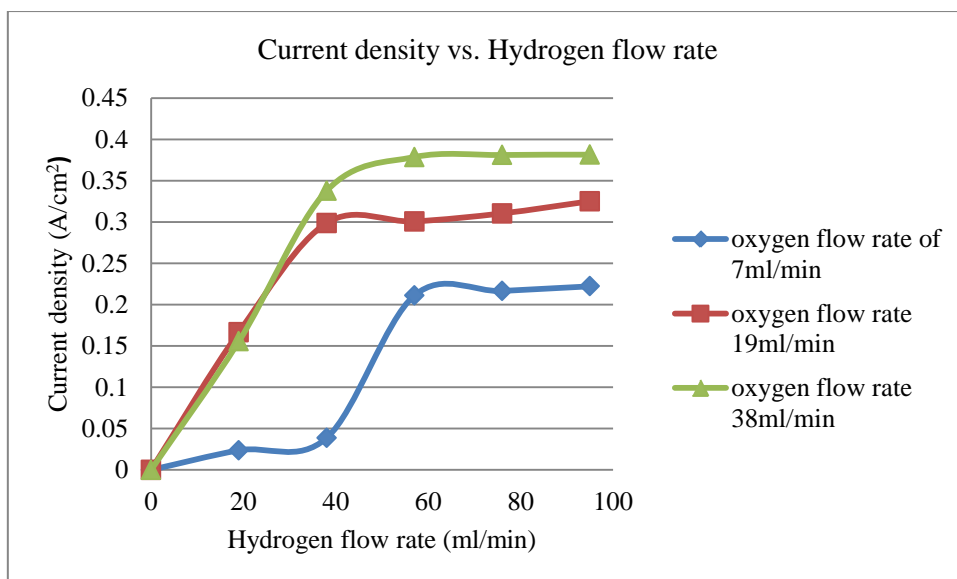
Figure 30: MEA 1, Current density at varying reactant flow rates

Table 12: MEA 2, current density at varying reactant flow rates

Hydrogen flow rate (ml/min)	Current density at oxygen flow rate of 7ml/min (A/cm^2)	Current density at oxygen flow rate 19ml/min (A/cm^2)	Current density at oxygen flow rate 38ml/min (A/cm^2)
0	0	0	0
19	0.1666	0.1888	0.1944
38	0.1888	0.2306	0.2726
57	0.1966	0.2325	0.2784
76	0.1977	0.2331	0.2833
95	0.1988	0.2333	0.284
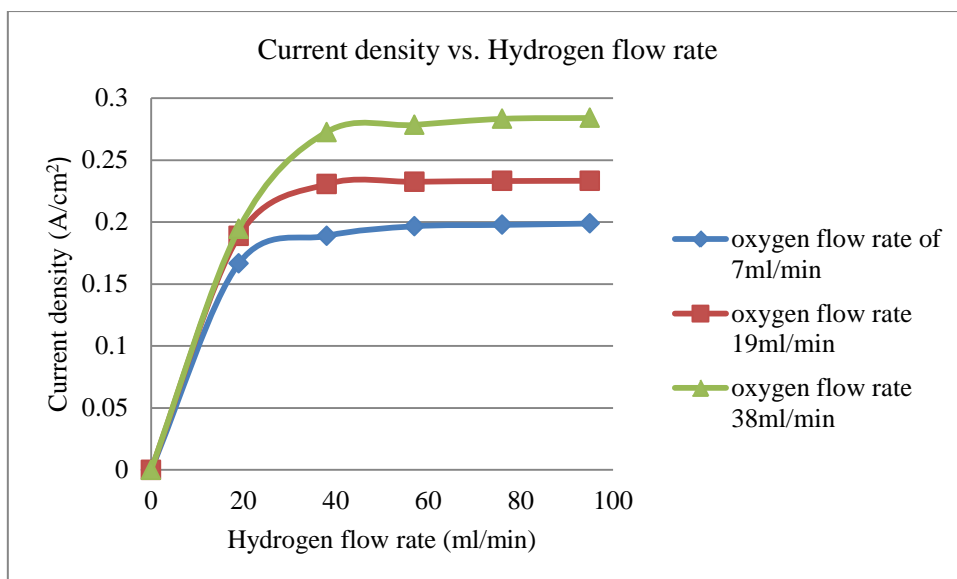
Figure 31: MEA 2, Current density at varying reactant flow rates

Table 13: MEA 1 vs. MEA 2, current density, varying H_2, O_2 7 ml/min

Hydrogen flow rate (ml\min)	Oxygen flow rate (ml\min)	MEA1 (A/cm^2)	MEA2 (A/cm^2)
0	7	0	0
19	7	0.0237	0.1666
38	7	0.0386	0.1888
57	7	0.2111	0.1966
76	7	0.2166	0.1977
95	7	0.2222	0.1988
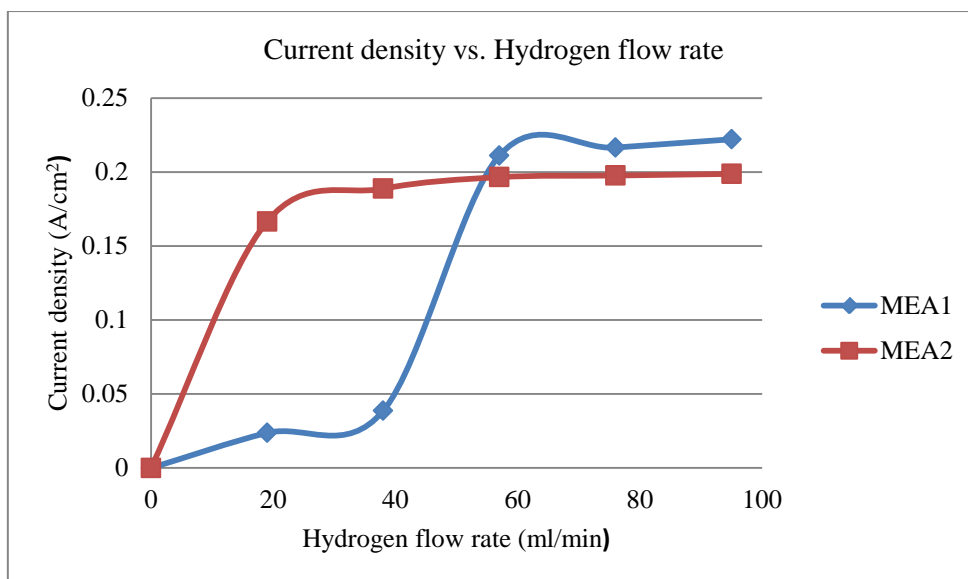
Figure 32: MEA 1 vs. MEA 2 current density, varying H_2, O_2 7 ml/min

Table 14: MEA 1 vs. MEA 2, current density, varying H_2, O_2 19 ml/min

Hydrogen flow rate (ml\min)	Oxygen flow rate (ml\min)	MEA1 (A/cm^2)	MEA2 (A/cm^2)
0	19	0	0
19	19	0.1666	0.1888
38	19	0.2988	0.2306
57	19	0.3008	0.2325
76	19	0.3105	0.2331
95	19	0.3252	0.2333
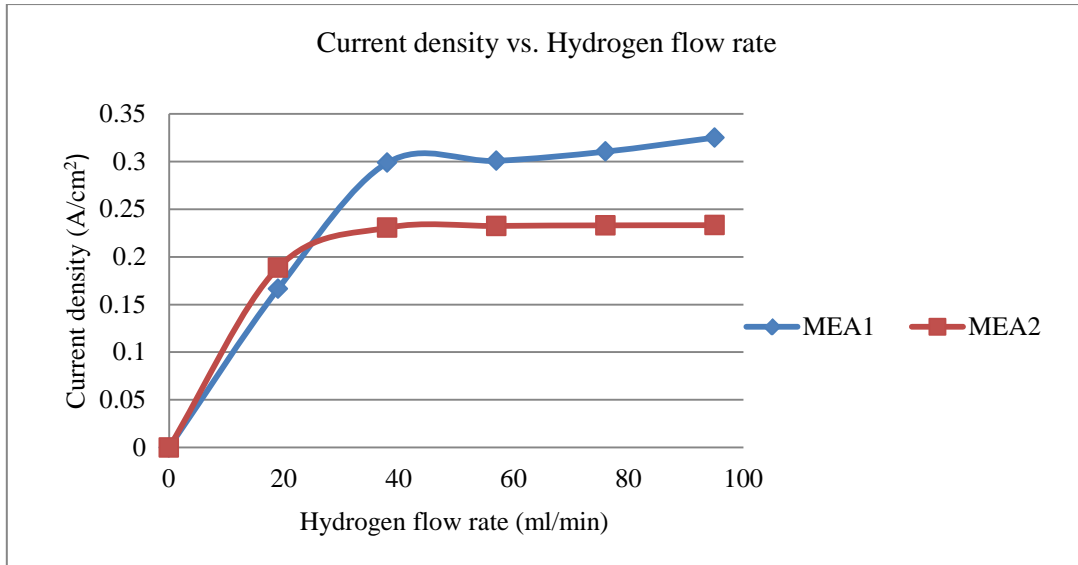
Figure 33: MEA 1 vs. MEA 2 current density, varying H_2, O_2 19 ml/min

Table 15: MEA 1 vs. MEA 2 vs. MEA 3 vs. MEA 4, current density, varying H_2, O_2 38 ml/min

Hydrogen flow rate (ml\min)	Oxygen flow rate (ml\min)	MEA1 (A/cm^2)	MEA2 (A/cm^2)	MEA3 (A/cm^2)	MEA4 (A/cm^2)
0	38	0	0	0	0
19	38	0.1555	0.1944	14.9 x 10^{-6}	41.3 x 10^{-6}
38	38	0.3378	0.2726	15.2 x 10^{-6}	46.6 x 10^{-6}
57	38	0.3787	0.2784	15.2 x 10^{-6}	48.8 x 10^{-6}
76	38	0.3812	0.2833	15.4 x 10^{-6}	55.5 x 10^{-6}
95	38	0.3816	0.284	15.5 x 10^{-6}	55 x 10^{-6}
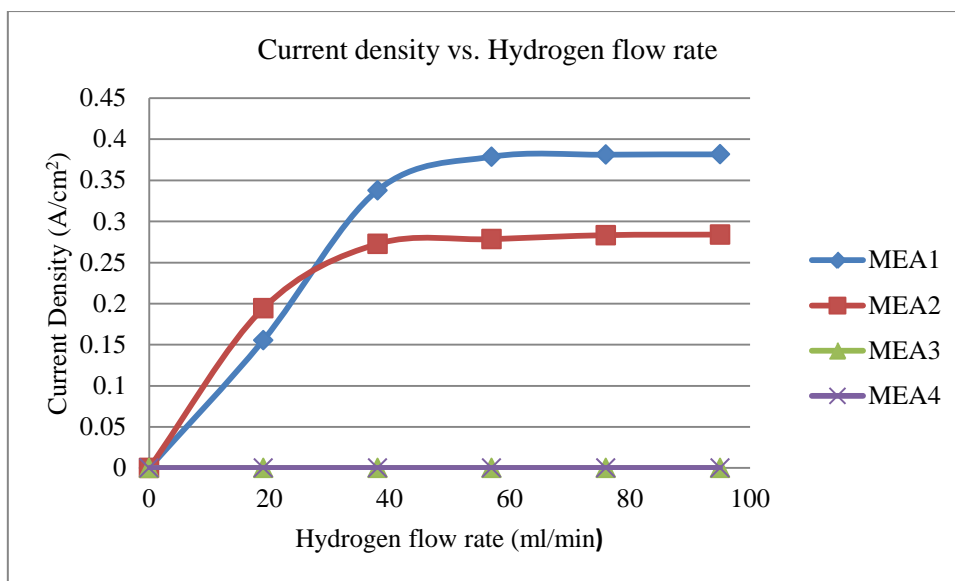
Figure 34: MEA 1 vs. MEA 2 vs. MEA 3 vs. MEA 4, current density, varying H_2, O_2 38 ml/min

Increasing reactant flow rate significantly improved the current density for MEA 1and 2. The maximum current density for MEA 1, 2, 3, and 4 were achieved when the highest flow rates were applied. This is due to more reactants being present at the reaction sites. Increasing reactant flow rate increases the reactant concentration at active catalyst sites thereby increasing the current density. However it can be seen above in Tables 11 – 15 that as the maximum current density is approached at a high flow rate, further increase in volume flow rate does not increase the current density. This shows that most of the active reaction zones are being utilized and that maximum current density is approached. MEA 1, 2, 3, 4 delivered a maximum current density of 0.3816, 0.284, 50×10^{-6} and 55×10^{-6} A/cm^2 respectively. Due to the porosity of the catalyst surface there is a possibility that the maximum current was not reached.

The 10.69 % difference in current density between MEA 1 and 2 at the highest flow rate is due to the increased platinum loading on MEA 1. Increasing the Pt loading increases the number of reaction sites available for the reactants to react with, thus increasing the output current. Increasing catalyst loading also increases the exchange current densities and increases the net current generated as shown above.

Poor current densities were achieved with MEA 3 and 4. Further increase in flow rate did not improve from its initial current density at low flow rates. It was noted that the current density initially peaked 133.3×10^{-6} A/cm^2 for MEA 3 and 247.8×10^{-6} A/cm^2 for MEA 4, and then slowly decreased whilst maintaining a constant reactant flow rate. The final value recorded

and provided was taken after 2 hours. The slow decrease in current density could be due to the possible formation of oxides on the catalyst surface, thus reducing the number of active sites for the reactants to react with, which significantly reduced the output current.

4.3 Polarization Curve

Table 16: MEA 1, power density and current density at 25°C and 35°C, H_2 19 ml/min, O_2 38 ml/min

Voltage (V)	MEA1 Current Density (A/cm^2) 25°C	MEA1 Current Density (A/cm^2) 35°C	MEA1 Power Density (W/cm^2) 25°C	MEA1 Power Density (W/cm^2) 35°C	Voltage Efficiency (%)
0.945	0	0	0	0	63.77
0.81	0.0047	0.0087	0.0037	0.0071	54.66
0.75	0.014	0.0164	0.0105	0.0123	50.61
0.67	0.0366	0.0472	0.0244	0.0316	45.21
0.56	0.0664	0.0871	0.0372	0.0487	37.79
0.48	0.0976	0.113	0.0468	0.0590	32.39
0.39	0.1298	0.155	0.0506	0.0604	26.32
0.304	0.148	0.187	0.0449	0.0568	20.51
0.24	0.192	0.2166	0.0460	0.0519	16.19
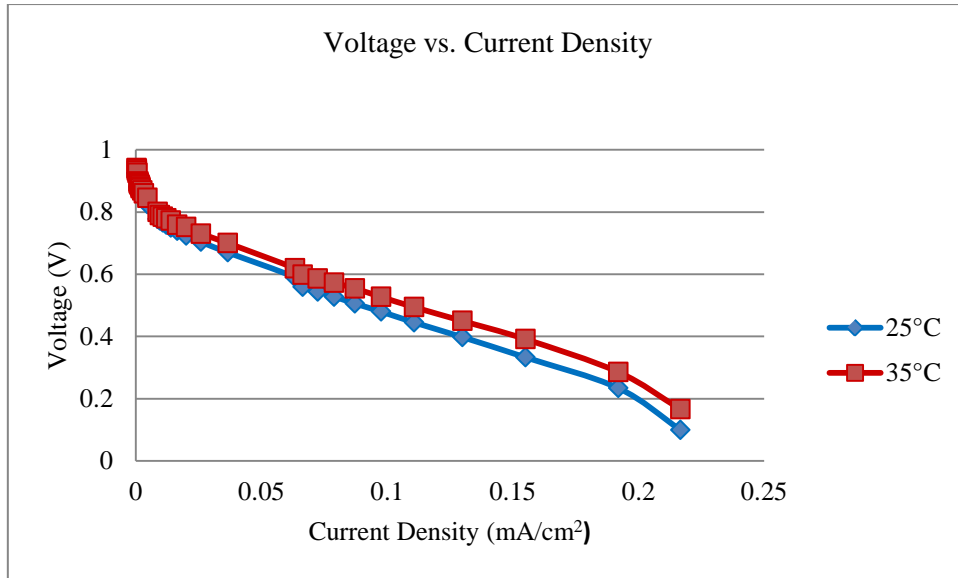
Figure 35: MEA 1, polarization curve at 25°C and 35°C, H$_2$ 19ml/min, O$_2$ 38ml/min

Table 17: MEA 2, power density and current density at 25°C and 35°C, H$_2$ 19ml/min, O$_2$ 38ml/min

Voltage (V)	MEA2 Current Density (A/cm^2) 25 °C	MEA2 Current Density (A/cm^2) 35 °C	MEA2 Power Density (W/cm^2) 25 °C	MEA2 Power Density (W/cm^2) 35 °C	Voltage Efficiency (%)
0.945	0	0	0	0	63.77
0.81	0.0013	0.0041	0.0011	0.0032	54.66
0.75	0.0032	0.0119	0.0024	0.0089	50.61
0.67	0.0121	0.0312	0.0081	0.0209	45.21
0.56	0.0378	0.0542	0.0212	0.0303	37.79
0.48	0.0633	0.0838	0.0303	0.0402	32.39
0.39	0.0939	0.1252	0.0366	0.0488	26.32
0.304	0.1275	0.1332	0.0387	0.0405	20.51
0.24	0.155	0.1673	0.0372	0.0401	16.19

53
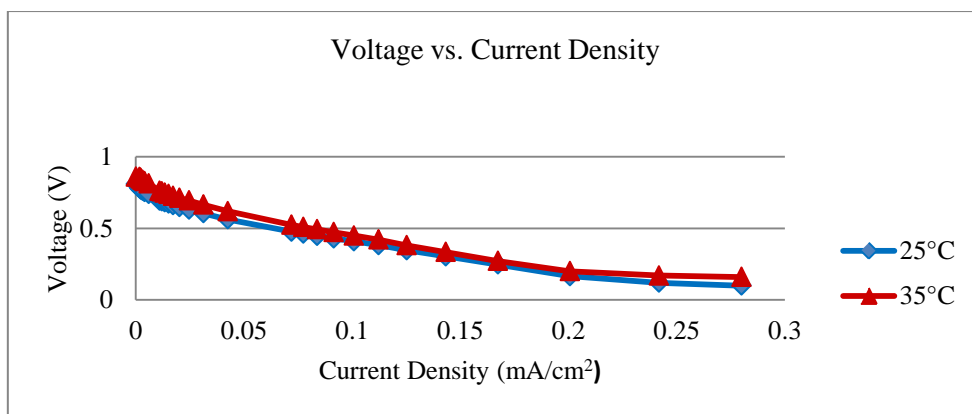
Figure 36: MEA 2 polarization curve at 25 °C and 35 °C, H_2 19 ml/min, O_2 38 ml/min
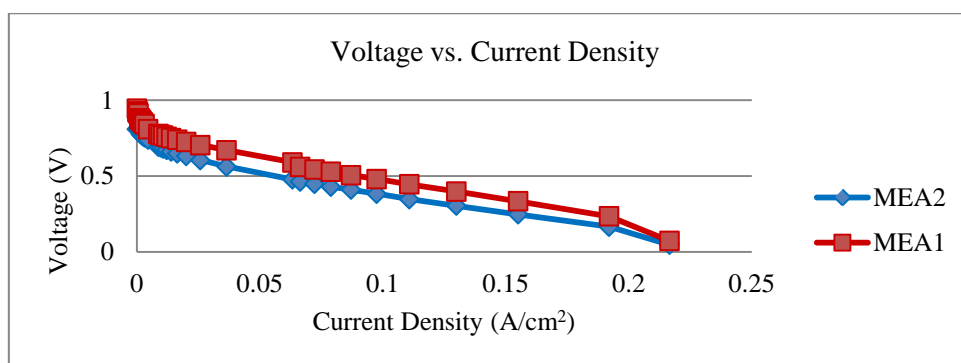
Figure 37: MEA 1 vs. MEA 2, polarization curve at 25 °C, H_2 19 ml/min, O_2 38 ml/min

Table 18: MEA 3, power density and current density at 25 °C and 35 °C, H_2 19 ml/min, O_2 38 ml/min

MEA3 Current Density ($\mu A/cm^2$) 25 °C	Voltage (V) 25 °C	Voltage (V) 35 °C	MEA3 Power Density ($\mu W/cm^2$) 25 °C	MEA3 Power Density ($\mu W/cm^2$) 35 °C	Voltage Efficiency (%) 25 °C	Voltage Efficiency (%) 35 °C
0	0.4556	0.4551	0	0	30.74	30.71
5.5556	0.3697	0.3784	2.0539	2.1022	24.95	25.53
6.667	0.3471	0.3514	2.3141	2.3427	23.42	23.71
7.778	0.2502	0.2598	1.9461	2.0207	16.88	17.53
8.889	0.2041	0.2101	1.8142	1.8675	13.77	14.18
11.11	0.0872	0.0921	0.9687	1.0231	5.88	6.21
12.22	0.0479	0.0524	0.5853	0.6403	3.23	3.54
13.33	0.0104	0.0134	0.1386	0.1786	0.7	0.9
13.33	0.0053	0.0064	0.0706	0.0853	0.36	0.43
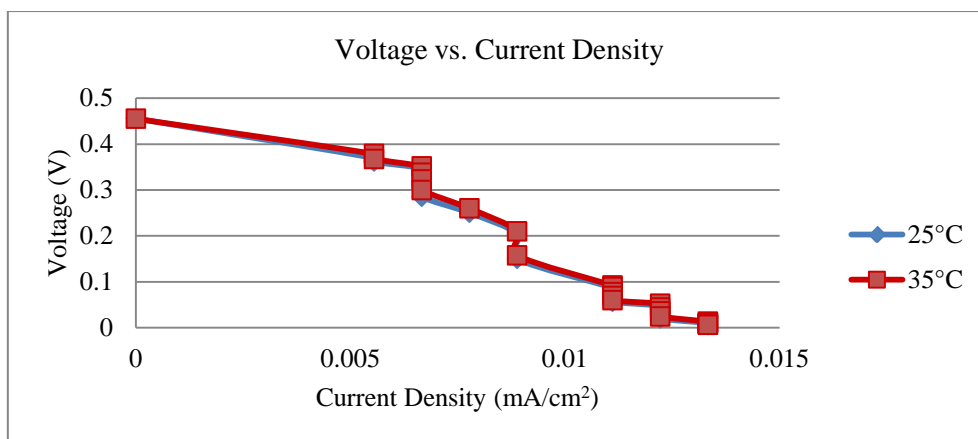
Figure 38: MEA 3, polarization curve at 25 °C and 35 °C, H$_2$ 19 ml/min, O$_2$ 38 ml/min

Table 19: MEA 4, power density and current density at 25 °C and 35 °C, H$_2$ 19 ml/min, O$_2$ 38 ml/min

MEA4 Current Density (μA/cm^2)	Voltage 25 °C (V)	Voltage 35 °C (V)	MEA4 Power Density (μW/cm^2) 25 °C	MEA4 Power Density (μW/cm^2) 35 °C	Voltage Efficiency (%) 25 °C	Voltage Efficiency (%) 35 °C
0	0.32	0.34	0	0	21.59	22.94
3.3333	0.2301	0.24	0.7669	0.7999	15.53	16.19
4.4444	0.2214	0.229	0.9839	1.0177	14.94	15.45
5.5556	0.208	0.215	1.1555	1.1944	14.04	14.51
6.6666	0.1905	0.204	1.2699	1.3599	12.85	13.77
7.77	0.1771	0.192	1.3760	1.4918	11.95	12.96
15.55	0.1283	0.142	1.9950	2.2081	8.66	9.85
26.66	0.0705	0.083	1.8795	2.2127	4.76	5.6
53.33	0.0015	0.0019	0.0799	0.1013	0.1	0.13
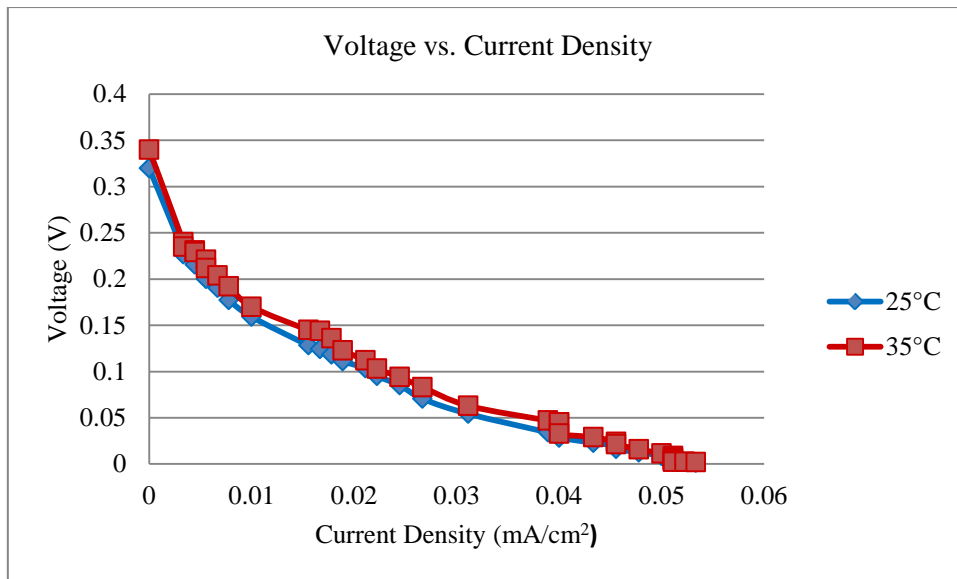
Figure 39: MEA 4, polarization curve at 25 °C and 35 °C, H_2 19 ml/min, O_2 38 ml/min

Voltage vs. current density plots were recorded at a constant hydrogen flow rate of 19 ml/min and oxygen flow rate of 38 ml/min at 25 °C and 35 °C. It can be seen from Figures 35 - 39 that a slight performance gain was achieved when the temperature was increased.

The low current density region in Figures 35 - 39 shows a sharp drop in potential, this is the activation energy required to start the reaction. Increasing temperature shows a decrease in the amount of activation losses which meant the reaction was able to precede at a faster rate hence less loss of potential from reaction kinetics. Increasing temperature also increases exchange current density as shown equation (12) which decreases the activation over potential.

The over potential losses in the intermediate current density region is attributed to ohmic losses which increase with current and temperature (see equation (13)). At higher temperature ohmic losses are increased due to membrane drying. Supplying humidified gases improves membrane conductivity which allows protons to be conducted more easily through the membrane and decrease its resistance, hence the decrease in ohmic losses in the intermediate region.

The high current density region shows a rapid decrease in cell potential due to concentration over potential which is expected as a result of reactant consumption at the catalyst site exceeding the rate of reactant diffusion. At higher temperature there is a decrease in

concentration over potential. Overall the cell performance increased at higher temperatures due to a decrease in losses.

4.4 Power Density
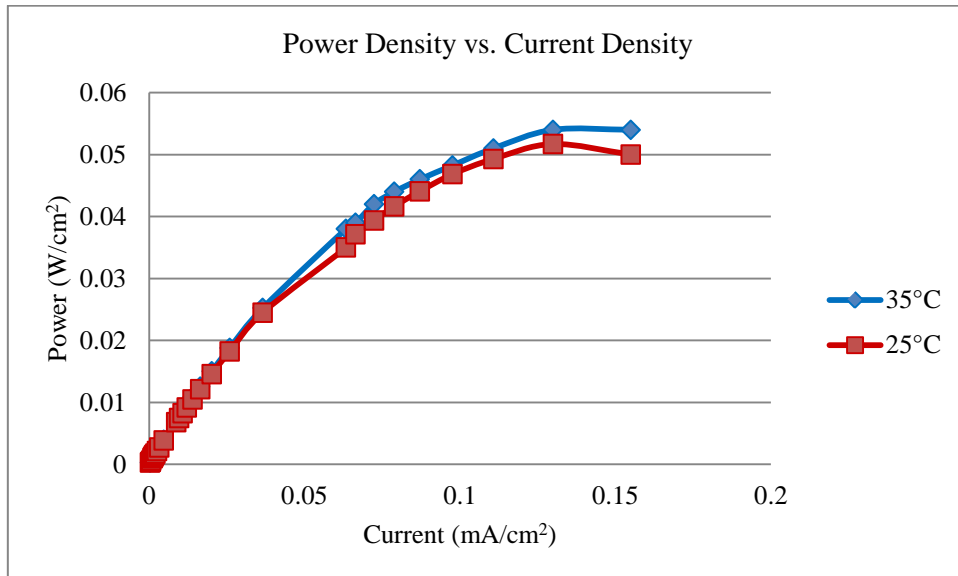
Figure 40: MEA 1, maximum power density at 25 °C and 35 °C, H_2 19 ml/min, O_2 38 ml/min
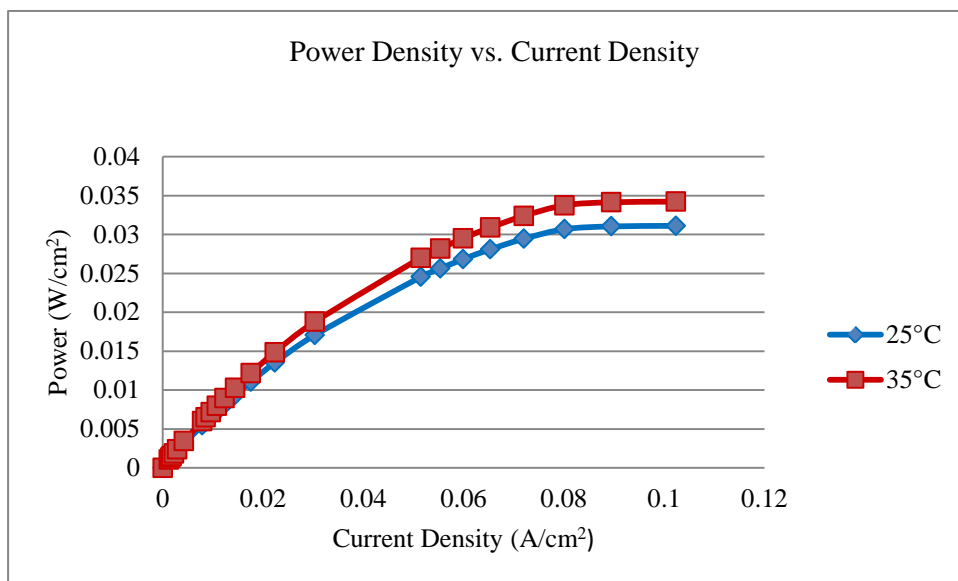
Figure 41: MEA 2, maximum power density at 25 °C and 35 °C, H_2 19 ml/min, O_2 38 ml/min
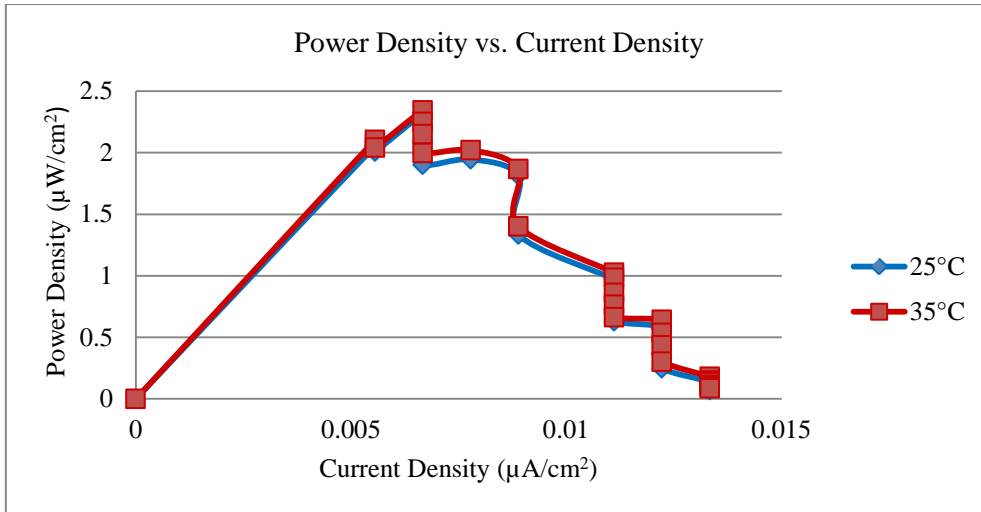
Figure 42: MEA 3, maximum power density at 25 °C and 35 °C, H_2 19 ml/min, O_2 38 ml/min
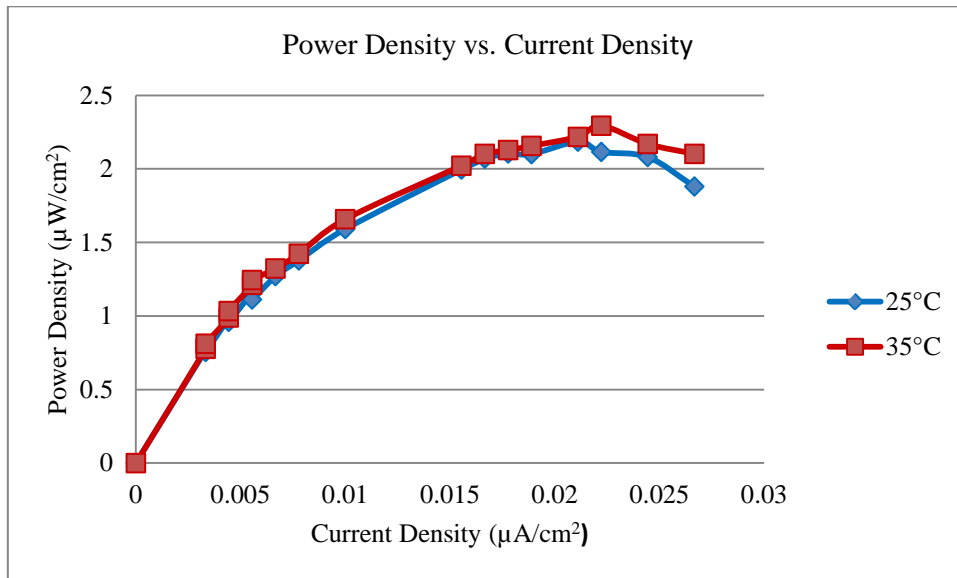
Figure 43: MEA 4, maximum power density at 25 °C and 35 °C, H_2 19 ml/min, O_2 38 ml/min
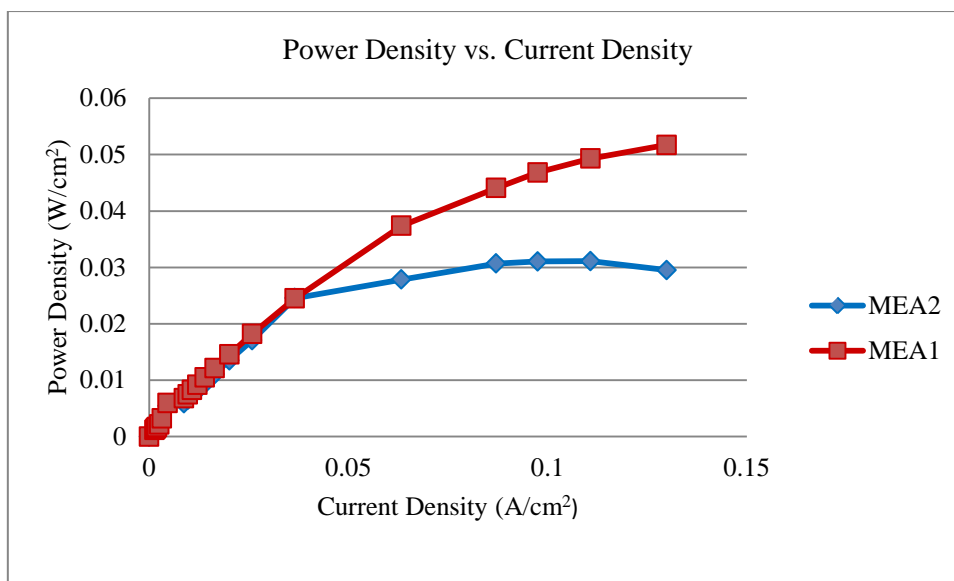
Figure 44: MEA 1 vs. MEA 2, maximum power density at 25 °C, H_2 19 ml/min, O_2 38 ml/min

The plots of power density vs. current density are shown in Figures 40 - 44. It can be seen from the figures that the power density has a fairly linear relationship with current density up to the maximum power point, further increase in current shows a drop in cell power density and this could be due to insufficient supply of hydrogen to the active area surface.

MEA 1, 2, 3, and 4 delivered a maximum power density of 0.05, 0.038, 2.3×10^{-6}, and 1.99×10^{-6} W/cm^2 respectively at 25 °C. The 10 °C increase in temperature increased the power delivered by the MEAs to 0.06, 0.0488, 2.342×10^{-6}, 2.212×10^{-6} W/cm^2. The slight increase in power density for the MEAs for a 10 °C temperature increase was expected. This is due to a higher current density being achieved with a lower overpotential as the reaction kinetics increased.

The significant decrease in power density for MEA 3 and 4 compared to MEA 1 and 2 is due to the poor exchange current density of the material. This results in higher over potentials and lower net output current due to reaction proceeding at a slower rate and the possible formation of oxides on the catalyst surface.

The 22.6 % difference in maximum power density between MEA 1 and 2 at 25 °C is due to the higher Pt loading on MEA 1 as discussed earlier which increases the exchange current density and current output at a given potential.

4.5 Cost vs. Maximum Power Density vs. Voltage Efficiency

Table 20: Cost vs. power density at 25 °C vs. voltage efficiency

MEA	Catalyst Cost (Rands)	Maximum Power Density(W/cm^2)	Voltage Efficiency (%)
1	1.549	0.0506	26.32
2	0.387	0.0387	20.51
3	0.21	2.314×10^{-6}	23.42
4	0.21	1.9951×10^{-6}	8.66

The cost of the catalyst and efficiency at maximum power density is shown in Table 20. It can be seen that at the maximum power density, efficiency is low. Higher efficiencies can be obtained at lower power density, however higher efficiency means operating the cell at a higher voltage. This implies increasing the number of cells to compensate for the increase in voltage. When a fuel cell stack is considered to obtain the same power output, costs increase. Fuel cell cost and efficiency are interrelated.

The significant cost and power density difference between the Pt and non Pt loaded MEAs shows that using the catalyst material combination in this study did not produced a reasonable power density for the lower cost.

4.6 Scanning electron microscope (SEM)

The images in Figures 45 - 49 show the particle morphologies and a fairly uniform dispersion onto the Nafion membrane. The particle size of Ag measured from the SEM image was 6.6µm.
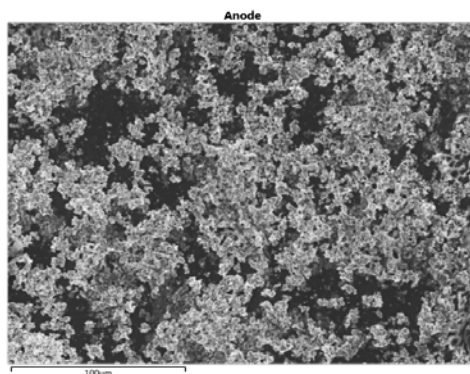
Figure 45: SEM of Ag dispersion on the anode

Ag Lα1
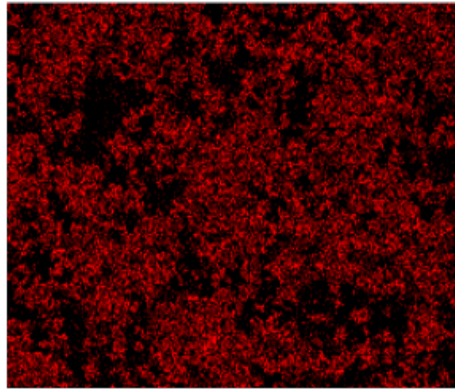
100µm

Figure 46: SEM of Ag colour dispersion on the anode

Cathode_1
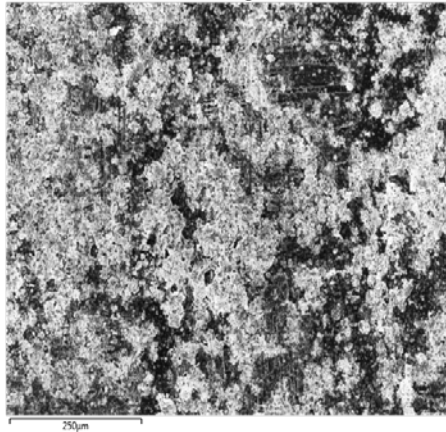
250µm

Figure 47: SEM of material combination dispersion on the cathode

Ag Lα1   **Ir Lα1**
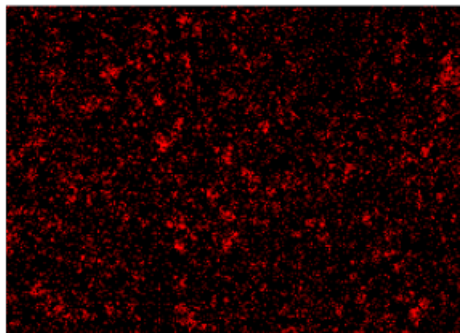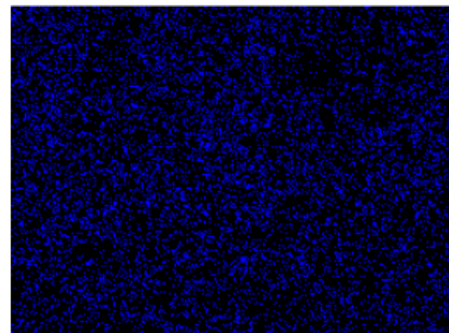
250µm   250µm

Figure 48: SEM of Ag and Ir dispersion on the cathode
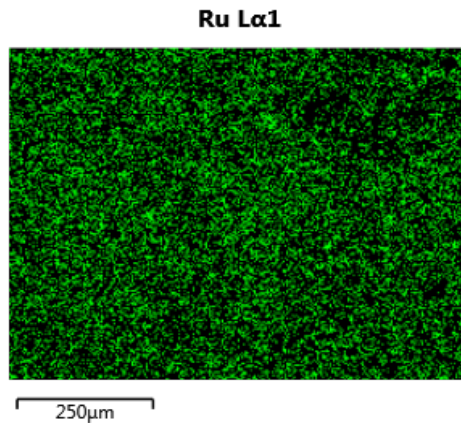
Figure 49: SEM of Ru dispersion on the cathode

4.7 Summary

In Chapter 4, the experiments carried out to monitor the performance of a non Pt coated catalyst against a Pt coated catalyst were presented. The maximum power density achieved by Pt based catalyst at 35 °C was 0.0604 W/cm^2 and 2.3427 μW/cm^2 for the non- Pt based MEA. The results showed that the material combination chosen in this work performed poorly and further research is required to develop a material combination to match the performance of a Pt based PEMFC.

In Chapter 5, conclusions based on the literature review, test cell design, experimental setup and results are presented.

Chapter 5: Conclusion and Recommendations

Research investigating the effectiveness of using a low cost catalyst material for hydrogen PEMFC was carried out and conclusions made are based on the literature review, test cell design and the experimental results obtained.

5.1 Conclusion

The work presented in this study addressed the basic PEMFC theory, construction of a PEMFC, the experimental setup and characterisation of the cell under no - load and loaded conditions. This chapter will summarise the literature review, construction and experimental setup, including the results of the experimental work.

The literature review conducted addressed the main topics and issues regarding hydrogen fed PEMFCs. These are the most commonly used fuel cells in the automotive industry as they can operate at low temperatures, have a high power density, and offer no carbon emissions. A typical PEMFC consists of a polymer electrolyte membrane which has platinum supported on carbon dispersed on either side. The electrochemical reaction takes place at the three phase zone - that is at the interface where the polymer electrolyte membrane, catalyst and carbon meet. A gas diffusion layer is then placed on either side of the membrane electrode assembly to conduct the electrons released. The flow field plates and end plates are then placed on the gas diffusion layer to provide an entry point and transport path to the three phase zone.

The maximum theoretical voltage that can be achieved at equilibrium is 1.23V using the Gibbs free energy. This value is positively affected by an increase in pressure, and negatively affected by increases in temperature. However the maximum theoretical voltage cannot be practically achieved due to activation over potentials which are required to start the electrochemical reaction. The choice of material and its associated exchange current density is the single most important factor that affects the amount of activation over potential and net current generated. Increases in operating parameters also reduce the amount of activation over potential which occurs at low current densities. Ohmic losses occur at intermediate current densities due to the flow of electrons through the electrically conductive fuel cell components and ions through the membrane. Dehydration of the membrane increases these losses. Fuel cells typically operate and achieve their maximum power density in this region.

A substantial amount of practical experience was gained in developing the test cell and experimental test station. The materials science laboratory is now equipped with a basic experimental test station for performance characterization of a fuel cell. The Smart - Trak mass flow controller adequately fulfilled its role for precise flow control. However the purchase of a temperature controlled humidifier and heating pads would allow for the quick characterisation of the cell to higher temperatures.

The cost effective construction of the fuel cell hardware and purchasing of commercial and custom MEAs is a solid starting point for fuel cell research where funding is limited. This allows one to concentrate on the specific problems associated with the test cell instead of designing and manufacturing each cell component. Simple issues like gasketing, cell compression, and proper electrical connection need attention to ensure a good operating test cell. The commercial MEA was used with the aim of achieving comparable results with other research to ensure the correct operating parameter setting and to test the custom MEA under similar conditions to monitor performance variation. PEMFC can operate at above atmospheric pressure and within the temperature limits of the polymer electrolyte membrane.

It had been hypothesized that using a low cost material combination for the catalyst layer would produce an acceptable amount of electrical energy. The maximum power density results obtained with the Pt catalyst were comparable to those achieved by other researchers which ensured that the test cell was well developed and that the experimental setup and operating parameter settings were correct. The custom made non Pt loaded catalyst performance was found to perform poorly against the commercial Pt loaded catalyst due to the much stronger adsorption and poor stability characteristics of the material combination considered. The open circuit voltage was expected, however the poor current density achieved needs further investigation. Characterization of the catalyst layer using appropriate testing methods are required to confirm the possible presence of oxides on the catalyst surface which could of significantly reduced the number of reaction zones thus decreasing the net current generated in this study. Investigations into the fine tuning of the electronic configurations of materials are also required to achieve the ideal catalyst.

Temperature effects limited to 35 °C and catalysts loading were investigated to show a trend in the performance improvement of the fuel cell. It was found that reaction kinetics are increased which reduces the amount of overpotentials and improves performance. However at

high temperatures, membrane drying is an issue and careful water management is required. Further research is required in membrane hydration at high temperature without the use of external humidification.

Effects of varying reactant flow rates were investigated in order to monitor the performance of the open circuit voltage and limiting current. It was found that increasing flow rates slightly improves open circuit voltage and increases current density due to the high concentration of reactants at the reaction zones.

The work done is this study covered a wide range of research topics; inevitably there will be some questions left that require further research. Overall, insightful knowledge of fuel cell design, experimental setup, testing methods, analysis and issues common to PEMFC were obtained. This knowledge allows for the formulation on an action plan and recommendations to address the problems experienced in this research.

5.2 Recommendations

The following recommendations are made:

- Investigate the possibility of developing novel electro catalysts where their electronic configurations are similar to metals with excellent electro - catalytic and stability characteristics.

- Operate the PEMFC at high temperatures to reduce the effects of oxide formation on the catalyst surface.

- Investigate the possibility of developing a hydrated membrane to deal with the issue of water management at high temperatures.

- Consider using a high surface area catalyst support such as carbon nano tubes (CNT) to increase the number of reaction zones.

- Invest in a humidification unit to ensure proper control of the humidification of reactant gases.

- Invest in heating pads for a quick increase of cell temperature.

REFERENCES

[1] Grove, William R, 'On Voltiac Series and the Combination of Gases by Platinum', Philosophical Magazine, February 1839, pp. 127-30.

[2] Jianlu Zhang, Huamin Zhang, Jinfeng Wu, Juijun Zhang, 'PEM Fuel Testing and Diagnosis', Elsevier Publishing 2013.

[3] Vladimir S. Bagotsky,' The Long History of Fuel Cells: Problems and Solutions', 2nd ed. John Wiley and Sons, 2012, NJ, USA.

[4] Appleby, A. J and Foulkes F. R, (1993), Fuel cell handbook, Krieger Publishing Co, Florida.

[5] Daouda Fofana, Sadesh Kumar Natarajan, Pierre Bénard, and Jean Hamelin,' High Performance PEM Fuel Cell with Low Platinum Loading at the Cathode Using Magnetron Sputter Deposition, ISRN Electrochemistry,Volume 2013 (2013), Article ID 174834, 6 pages, 25 November 2012.

[6] Elizabeth Stockton Howard, 'The Design of Optimal Material Combinations for the Membrane Electrode Assembly of a Proton Exchange Membrane Fuel Cell', Bachelor of Science in Engineering Degree, Princeton University, 2006.

[7] JY Kim,T Oh, Y Shin, J Bonnett, K Scott Weil, 'A novel non platinum group electrocatalyst for the PEM cell application, International journal of hydrogen energy, 2010.

[8] Bossell U,' The birth of the Fuel Cell 1835–1845', Power for the 21st century 2004; 1:7.

[9] Rahul Mahtani, 'Investigating The Use Of Hydrogen As An Alternative Fuel', Degree of Bachelor of Science in Mechanical Engineering, WORCESTER POLYTECHNIC INSTITUTE, 2010.

[10] James Larminie, Andrew Dicks, 'Fuel Cell Systems Explained', second edition, John Wiley and Sons, The Atrium, Southern Gate, Chichester, West Sussex PO198SQ, England

[11] Colleen Spiegel, 'Designing and Building Fuel Cells', 1st ed. New York, NY, McGraw-Hill, 2007

[12] Rabir,S, Ralliers O, Turpin C, Astier S, 'Experimental study of a reversible fuel cell, University of Toulouse-Laboratory Laplace, 1:1-6.

[13] www.infomine.com, accessed 10 October 2015.

[14] Frano Barbir, 'PEM Fuel Cells: Theory and Practice', United States of America, Elsevier, 2005.

[15] www.heliocentric.com, accessed 15 July 2014.

[16] S. Litster, G. McLean,' Review PEM fuel cell electrodes, Journal of Power Sources 130 (2004) 61–76, 14 December 2003.

[17] Zhu Chen, Drew Higgins, Haisheng Tao, Ryan S. Hsu, and Zhongwei Chen, 'Highly Active Nitrogen–Doped Carbon Nanotubes for Oxygen Reduction in Fuel Cell Applications', Department of Chemical Engineering, Waterloo Institute for Nanotechnology, Waterloo Institute for Sustainable Energy, University of Waterloo, Ontario, Canada, September 27, 2009.

[18] Olivier T. Holton and Joseph W. Stevenson, 'Evaluation of Platinum's Unique Properties for Use in Both the Anode and Cathode of a Proton Exchange Membrane', Johnson Matthey, Orchard Road, Royston, Hertfordshire SG8 5HE, UK, 2013.

[19] Jiujun Zhang,'PEM Fuel Cell Electrocatalyst and Catalyst Layers', London, Springer, 2008.

[20] Cheng J, 'Study of IrxRu1−xO2 oxides as anodic electrocatalysts for solid polymer electrolyte water electrolysis', Electrochimica Acta, 2009. 54(26): p. 6250-6256.

[21] S.M.J. Zaidi, T. Matsuura (eds.) Polymer Membranes for Fuel Cells, Springer Science Business Media, LLC 2009.

[22] Van Tonder,'Optimization of Water Management for Reversible Fuel Cell', Master's Thesis, Vaal University of Technology, 2011.

[23] Mengbo Ji and Zidong Wei, 'A Review of Water Management in Polymer Electrolyte Membrane Fuel Cells', State Key Laboratory of Power Transmission Equipment & System Security and New Technology, School of Chemistry and Chemical Engineering, Chongqing

University, Chongqing, 400044, China, Received: 4 September 2009 / Accepted: 11 November 2009 / Published: Energies November 2009.

[24] EC Kumbur and MM Mench,' Water Management', The Pennsylvania State University, University Park, PA, USA, 2009 Elsevier B.V. All rights reserved.

[25] Heinzel, A., Mahlendor, A. & Jansen, C. 2009. Bipolar plates. Encyclopaedia of Electrochemical Power Sources, pp 810- 816.

[26] X. Li., I. Sabir, 2005. Review of bipolar plates in PEM fuel cells: Flow-field designs. International Journal of Hydrogen Energy. 30(4):359-371.

[27] D.H. Jeon, S.Greenway, S.Shimpalee, J.W. Van Zee, 'The effect of serpentine flow – field designs on PEM fuel cell performance', Department of Chemical Engineering, University of South Carolina, Columbia, 14 June 2007.

[28] Tuomas Mennola.' Design and Experimental Characterization of Polymer Electrolyte Membrane Fuel Cells', degree of Licentiate of Technology, Helsinki University of Technology, 2003.

[29] Doddathimmaiah, A. K. 2006.' The use of PEM unitised regenerative fuel cells in solar-hydrogen systems for remote area power supply'. School of Aerospace, Mechanical and Manufacturing; RMIT University.

[30] A. Husar, S. Strahl, J. Riera, 'Experimental Characterization Methodology for the Identification of Voltage Losses of PEMFC: Applied to an Open Cathode Stack', Institut de Robòtica i Informàtica Industrial (CSIC-UPC).

[31] Tuomas Mennola, , Mikko Mikkola, Matti Noponen, Tero Hottinen, Peter Lund, 'Measurement of ohmic voltage losses in individual cells of a PEMFC stack', Laboratory of Advanced Energy Systems, Helsinki University of Technology, P.O. Box 2200, FIN-02015 HUT, Espoo, Finland, Received 12 February 2002, Revised 12 July 2002, Accepted 15 July 2002, Available online 21 August 2002.

[32] Lin Wang, Attila Husar, Tianhong Zhou, Hongtan Liu,' A parametric study of PEM fuel cell performances', Department of Mechanical Engineering, University of Miami, 208

McArthur Engineering Bldg., Coral Gables, FL 33124, USA International Journal of Hydrogen Energy 28 (2003) 1263–1272.

[33] Mehdi Amirinejada, Soosan Rowshanzamirb, Mohammad H. Eikanic, 'Effects of operating parameters on performance of a proton exchange membrane fuel cell', Department of Chemical Engineering, School of Engineering, Razi University, Kermanshah, Iran, Department of Chemical Engineering, Iran University of Science and Technology (IUST), Tehran, Iran, Chemical Industries Research Center, Iranian Research Organization for Science and Technology (IROST), P.O. Box 15815-3538, Tehran, Iran, Received 26 November 2005, Revised 8 March 2006, Accepted 30 April 2006, Available online 22 June 2006.

[34] US Fuel Council's Single Cell Testing Task Force, 'Single Cell Test Protocol', Washington ,DC, July 13, 2006.

[35] X.Z. Yuan, S. Zhang, J.C. Sun, H. Wang,'A review of accelerated conditioning for a polymer electrolyte membrane fuel cell',J Power Sources, 196 (2011), pp. 9097–9106, Volume 38, Issue 23, 6 August 2013, Pages 9819–9825.

[36] Mohammad Zhiani,, Somayeh Majidi, 'Effect of MEA conditioning on PEMFC performance and EIS response under steady state condition', International Journal of Hydrogen Energy, Volume 38, Issue 23, 6 August 2013, Pages 9819–9825.

[37] C. Yang, M. Hu, C. Wang, G. Cao, 'A three-step activation method for proton exchange membrane fuel cells', J Power Sources, 197 (2012), pp. 180–185.

[38] Valter Bruno Reis e Silva, 'Polymer Electrolyte Membrane Fuel Cells: Activation Analysis and Operating Conditions Optimization', Doctor of Philosophy in Chemical and Biological Engineering, Porto University, August 2009.

[39] Peakscientific Precision hydrogen100, Instruction manual, 2014, www.peakscientific.com, last accessed 11 November 2014.

[40] Sierra Smart-Trak 2 Series 100 Mass Flow Meters and Controllers, Instruction manual, Revised January 2011, www.sierrainstruments.com, last accessed 20 January 2015.

Standard thermodynamic properties of chemical substances   ANNEXURE A

Molecular formula	Name	ΔH (kJ mol^{-1})			ΔG (kJ mol -1)		
		Crys.	Liq.	Gas	Crys.	Liq.	Gas
H_2O	Water		-285.8	-241.8		-237.1	-228.6
H_2O_2	Hydrogen peroxide		-187.8	-136.3		-120.4	-105.6
H_2O_2Sn	Tin(II) hydroxide	-561.1			-491.6		
H_2O_2Sr	Strontium hydroxide	-959.0					
H_2O_2Zn	Zinc hydroxide	-641.9			-553.5		
H_2O_3Si	Metasilicic acid	-1188.7			-1092.4		
H_2O_4S	Sulfuric acid		-814.0			-690.0	
H_2O_4Se	Selenic acid	-530.1					
H_2S	Hydrogen sulfide			-20.6			-33.4
H_2S_2	Hydrogen disulfide		-18.1	15.5			
H_2Se	Hydrogen selenide			29.7			15.9
H_2Sr	Strontium hydride	-180.3					
H_2Te	Hydrogen telluride			99.6			
H_2Th	Thorium hydride	-139.7			-100.0		
H_2Zr	Zirconium(II) hydride	-169.0			-128.8		
H_3N	Ammonia			-45.9			-16.4
H_3NO	Hydroxylamine	-114.2					
H_3O_2P	Hypophosphorous acid	-604.6	-595.4				
H_3O_3P	Phosphorous acid	-964.4					
H_3O_4P	Phosphoric acid	-1284.4	-1271.7		-1124.3	-1123.6	
H_3P	Phosphine			5.4			13.4
H_3Sb	Stibine			145.1			147.8
H_3U	Uranium(III) hydride	-127.2			-72.8		
H_4IN	Ammonium iodide	-201.4			-112.5		
H_4N_2	Hydrazine		50.6	95.4		149.3	159.4
$H_4N_2O_2$	Ammonium nitrite	-256.5					
$H_4N_2O_3$	Ammonium nitrate	-365.6			-183.9		
H_4N_4	Ammonium azide	115.5			274.2		
H_4O_4Si	Orthosilicic acid	-1481.1			-1332.9		
$H_4O_7P_2$	Pyrophosphoric acid	-2241.0	-2231.7				
H_4P_2	Diphosphine		-5.0	20.9			
H_4Si	Silane			34.3			56.9
H_4Sn	Stannane			162.8			188.3
H_5NO	Ammonium hydroxide		-361.2			-254.0	
H_5NO_3S	Ammonium hydrogen sulfite	-768.6					

Precision Hydrogen
Hydrogen Generator for GC

Part Number : See Reverse   Service Kit : 0B-3609

PEAK SCIENTIFIC

Your local gas generation partner

Description

The Precision Hydrogen generators are designed to provide the gas needed for detectors requiring Hydrogen fuel gas, such as FID and FPD. One generator is capable of supplying multiple detectors, and are available in various flow rates to ideally suit individual customers' needs.

These generators utilise a Proton Exchange Membrane to create the Hydrogen gas from deionized water, and a desiccant filtration stage is used to dry the gas.

Precision Hydrogen gas generators come with various safety features as standard, giving you complete peace of mind in the laboratory and a far safer, dependable and more convenient alternative to cylinder gas.

Applications

- **Detector Gas**
  - Fuel Gas

Key Features

- Suitable for fuel gas at standard detection limits
- 99.9995% Purity
- Internal leak detection with automatic shutdown features
- Automatic loading pump as standard
- Simple maintenance, limited to replacing de-ionizer cartridge and silica gel
- Short and easy start-up and shutdown procedures
- Compact, space-saving modular design
- Creates hydrogen on demand, minimal storage of hydrogen in the system
- Peak offers a 3 year cell warranty with this generator as standard.
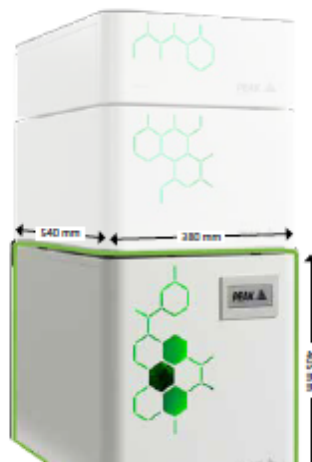
Precision Hydrogen shown in a typical Precision stack.

PEAK SCIENTIFIC

Technical Specifications	Hydrogen, 100cc	Hydrogen, 200cc	Hydrogen, 300cc	Hydrogen, 450cc
Max Flow Rate	100cc/min	200cc/min	300cc/min	450cc/min
Max Pressure	100 psi / 6.9 bar			
Purity	99.9995%			
Gas Outlets	1x 1/8" Swagelok compression fitting			
Water Purity Requirement	<1.0μ Siemens/cm OR >1 Mohm-cm			
Water Consumption	up to 0.12L/ day	up to 0.24L/day	up to 0.36L/day	up to 0.53L/day
Operating Temperature	10°C - 35°C / 50°F - 95°F			
Electrical Requirements	110-230V 50/60HZ 6A			
Power Consumption	660 watts - 1380 watts			
Heat Output	up to 4706 BTU/hr			
Generator Dimensions	38.0x 54.0 x 40.6cm / 14.9x 21.2x 15.9"			
Generator Weight	29 Kg (64 lbs)			
Noise Level	Silent in operation			

Ordering Information				
Part Number	63-0100	63-0200	63-0300	63-0450
Annual Service	08-3609			
Standard Maintenance Plan	09 - 3110			
Complete Maintenance Plan	09 - 3010			

Accessories	Water Bottle 4L	Water Bottle 8L
Water Bottle 4L	10-9016	10-9017

[PEAK Protected]™

Peak Scientific gas generators define the benchmark in reliability, convenience and performance in laboratories around the world, and come backed by a 12 month warranty. Beyond this period however you can ensure that you're investment continues to be [Protected] by our comprehensive generator care cover.

Our world-class aftercare support packages deliver a program of scheduled preventative maintenance whilst giving you the reassurance of instant access to worldwide technical support and priority on-site response in the untimely event of a breakdown.

Example of Smart -Trak 2 Data Labels   ANNEXURE C

<table>
<tr><td colspan="3">SIERRA INSTRUMENTS, INC. THE MASS FLOW COMPANY CE</td><td>5 Harris Court Bldg. L
Monterey, Ca. 93940
800-866-0200
831-373-0200</td></tr>
<tr><td colspan="4" align="center">Mass Flow Controller</td></tr>
<tr><td colspan="4" align="center">Model</td></tr>
<tr><td colspan="4" align="center">C100L-L-DD-LE-5-OV1-SV1-PV1C-V1-S1</td></tr>
<tr><td>Serial</td><td>Order</td><td colspan="2">Mfg. Date</td></tr>
<tr><td>10067</td><td>10001</td><td colspan="2">7/1/03</td></tr>
<tr><td colspan="4" align="center">Gas</td></tr>
<tr><td colspan="4" align="center">Air</td></tr>
<tr><td colspan="2">Range & Units</td><td colspan="2">STP</td></tr>
<tr><td colspan="2">0-1 SLPM</td><td colspan="2">70F / 1 ATM</td></tr>
<tr><td colspan="2">Output Signal</td><td colspan="2">Set Signal</td></tr>
<tr><td colspan="2">0-5 Vdc</td><td colspan="2">0-5 Vdc</td></tr>
<tr><td colspan="2">Orientation</td><td colspan="2">Supply</td></tr>
<tr><td colspan="2">Horizontal</td><td colspan="2">12-15 Vdc</td></tr>
<tr><td>Inlet Press.</td><td>Outlet Press.</td><td colspan="2">Max. Press.</td></tr>
<tr><td>30 PSI</td><td>ATM</td><td colspan="2">500 PSIG</td></tr>
<tr><td>Oper. Temp</td><td>Max. Temp</td><td colspan="2">Connections</td></tr>
<tr><td>70F</td><td>122F</td><td colspan="2">1/4" VCO</td></tr>
<tr><td colspan="2">O-ring Material</td><td colspan="2">Valve Seat Material</td></tr>
<tr><td colspan="2">Viton</td><td colspan="2">Viton</td></tr>
<tr><td>Technician</td><td>Cal. Date</td><td colspan="2">Recal. Date</td></tr>
<tr><td></td><td></td><td colspan="2"></td></tr>
<tr><td colspan="4" align="center">www.sierrasmarttrak.com</td></tr>
<tr><td colspan="2">Made in USA</td><td colspan="2">ISO 9001 Registered</td></tr>
</table>

<table>
<tr><td colspan="3">SIERRA INSTRUMENTS, INC. THE MASS FLOW COMPANY CE</td><td>5 Harris Court Bldg. L
Monterey, Ca. 93940
800-866-0200
831-373-0200</td></tr>
<tr><td colspan="4" align="center">Mass Flow Meter</td></tr>
<tr><td colspan="4" align="center">Model</td></tr>
<tr><td colspan="4" align="center">M100L-L-DD-LE-5-OV1-SV1-PV2-V4-S4</td></tr>
<tr><td>Serial</td><td>Order</td><td colspan="2">Mfg. Date</td></tr>
<tr><td>10068</td><td>10001</td><td colspan="2">7/1/03</td></tr>
<tr><td colspan="4" align="center">Gas</td></tr>
<tr><td colspan="4" align="center">Nitrogen</td></tr>
<tr><td colspan="2">Range & Units</td><td colspan="2">STP</td></tr>
<tr><td colspan="2">0-1 NM3/hr</td><td colspan="2">21C/760 mmHg</td></tr>
<tr><td colspan="2">Output Signal</td><td colspan="2">Set Signal</td></tr>
<tr><td colspan="2">4-20 mA</td><td colspan="2">4-20 mA</td></tr>
<tr><td colspan="2">Orientation</td><td colspan="2">Supply</td></tr>
<tr><td colspan="2">Vertical Flow Down</td><td colspan="2">24-30 Vdc</td></tr>
<tr><td>Inlet Press.</td><td>Outlet Press.</td><td colspan="2">Max. Press.</td></tr>
<tr><td>2 BARG</td><td>ATM</td><td colspan="2">35 BARG</td></tr>
<tr><td>Oper. Temp</td><td>Max. Temp</td><td colspan="2">Connections</td></tr>
<tr><td>20C</td><td>50C</td><td colspan="2">3/8 VCR</td></tr>
<tr><td colspan="2">O-ring Material</td><td colspan="2">Valve Seat Material</td></tr>
<tr><td colspan="2">Viton</td><td colspan="2">Viton</td></tr>
<tr><td>Technician</td><td>Cal. Date</td><td colspan="2">Recal. Date</td></tr>
<tr><td></td><td></td><td colspan="2"></td></tr>
<tr><td colspan="4" align="center">www.sierrasmarttrak.com</td></tr>
<tr><td colspan="2">Made in USA</td><td colspan="2">ISO 9001 Registered</td></tr>
</table>

Figure 2-4: Wiring Definitions for Optional Communication Cable

Pin #	Wire Color in Cable	Function
1.	Brown	Analog Ground/Output
2.	Red	0-5 VDC Output (or 0-10, 1-5 VDC)
3.	Orange	Analog Ground/RS232
4.	Pink	Valve Override Purge
5.	Yellow	Power Return (-)
6.	Green	Power Input (+)
7.	Green/White	RS-232 Transmit (out)
8.	Blue	Setpoint
9.	Purple	Not Used
10.	Gray	Analog Ground/Setpoint
11.	White	Reference Voltage (5 VDC External Setpoint & Valve Purge)
12.	Black	Valve Override Close
13.	Brown/white	RS-232 Receive (in)
14.	Red/white	4-20 mA Output
15.	Red/Black	Not Used
	Shield Wire (no insulation)	Chassis (Earth) Ground

Note: Pins 1, 3, and 10 are connected together inside the instrument. Do not tie these grounds together outside the instrument. Must have one connection per analog ground. Recommended use listed.

M100L & C100L Front View
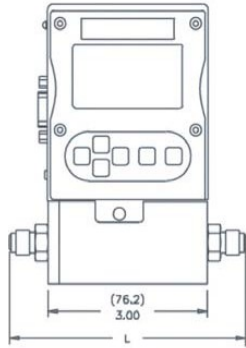
M100L & C100L Inlet View
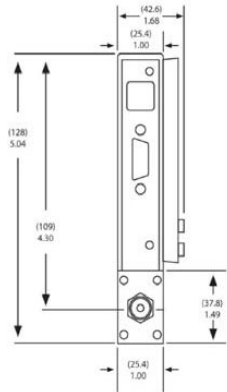
M100M Front View
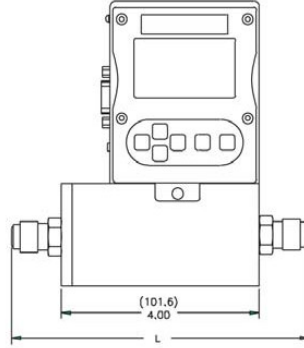
M100M Inlet View
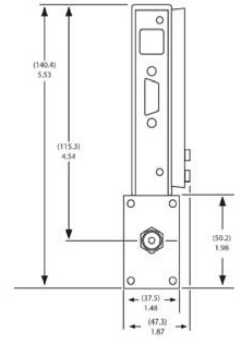
M100L & C100L Bottom View

C100M Front View

C100M Inlet View
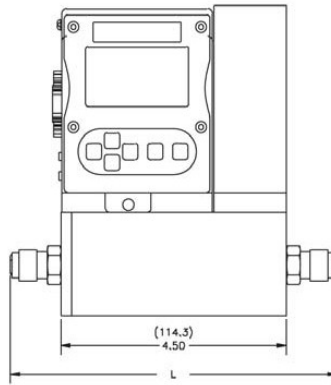
M100M & C100M Bottom View
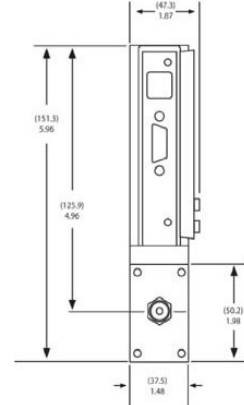
C100H1,H2 Front View   C100H1,H2 Side View   C100H1,H2 Bottom View
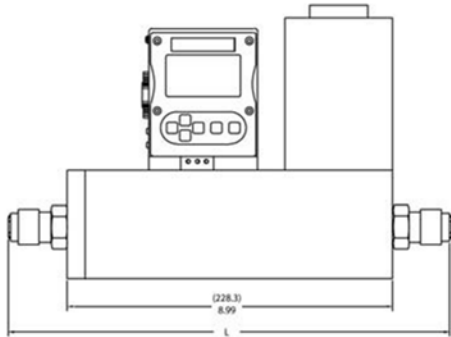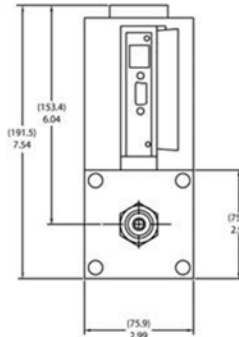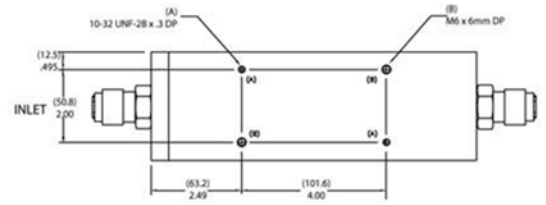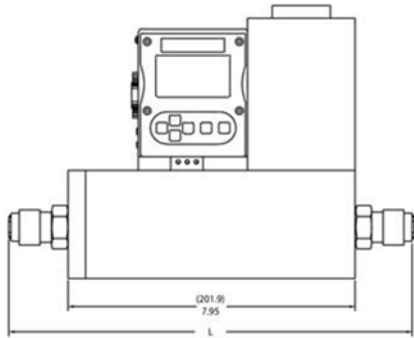
C100H Front View   C100H Side View   C100H Bottom View
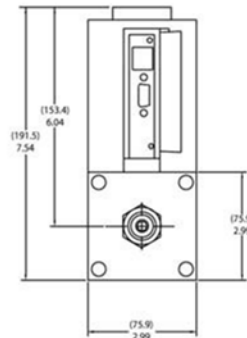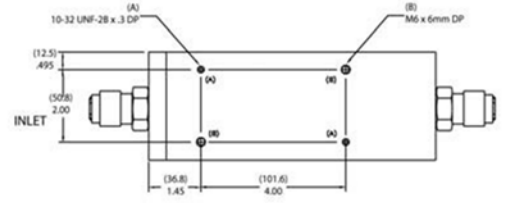
M100H,H1,H2 Front View   M100H,H1,H2 Side View   M100H,H1,H2 Bottom View
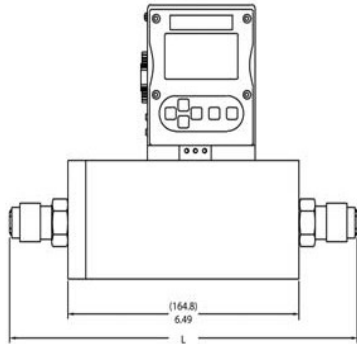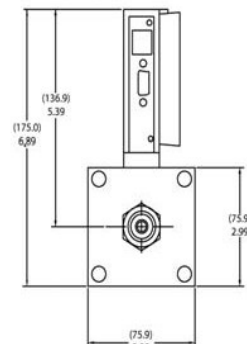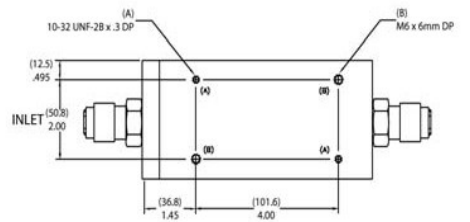
Dimension L

Fittings	Length with fittings in inches (mm)						
	C100L/M100L	C100M	M100M	M100H	M100H1, H2	C100H	C100H1, H2
1/8 compression	4.84 (124)	NA	NA	NA	NA	NA	NA
¼ compression	5.02 (129)	6.52 (167)	6.02 (154)	NA	NA	NA	NA
3/8 compression	5.14 (132)	6.64 (170)	6.14 (157)	NA	NA	NA	NA
½ compression	5.3 (136)	6.80 (174)	6.30 (162)	8.92 (229)	NA	10.37 (266)	NA
¼ VCO	4.56 (117)	6.06 (155)	5.56 (143)	NA	NA	NA	NA
½ VCO	5.00 (128)	6.50 (167)	6.00 (154)	8.56 (220)	NA	10.01 (257)	NA
¾ VCO	NA	NA	NA	NA	8.78 (225)	NA	11.28 (289)
¼ VCR	4.88 (125)	6.38 (164)	5.88 (151)	NA	NA	NA	NA
½ VCR	5.18 (133)	6.68 (171)	6.18 (158)	8.98 (230)	NA	10.43 (267)	NA
6 mm compression	5.04 (129)	6.54 (168)	6.04 (155)	NA	NA	NA	NA
10 mm compression	5.20 (133)	6.70 (172)	6.20 (159)	NA	NA	NA	NA
12 mm compression	5.38 (138)	6.88 (176)	6.38 (164)	8.90 (228)	NA	10.35 (265)	NA
¼ FNPT	4.85 (124)	6.35 (163)	5.85 (150)	NA	NA	NA	NA
3/8 FNPT	NA	6.50 (167)	6.00 (154)	NA	NA	NA	NA
½ FNPT	NA	NA	NA	9.14 (234)	NA	10.59 (272)	NA
¾ FNPT	NA	NA	NA	NA	9.30 (238)	NA	11.80 (303)
¾ compression	NA	NA	NA	9.24 (237)	9.18 (235)	10.69 (274)	11.68 (300)
1 inch compression	NA	NA	NA	NA	9.52 (244)	NA	12.02 (308)

78